UNIVERSITÀ DEGLI STUDI DI PADOVA

Dipartimento di Ingegneria Industriale

Corso di Laurea Magistrale in
Ingegneria dei Materiali

"Structured Li$_2$SO$_4$-Na$_2$SO$_4$ components for thermal energy storage "

Relatore:
Prof. Giorgia Franchin

Co-relatore:
Dr. Ali Ezzine

Laureando:
Matteo Bertoldi
Matricola 2022267

Anno accademico:
2022/2023

Abstract

The two salts are Li_2SO_4 and Na_2SO_4. They are two ternary salts that, when used together, create the Li_2SO_4-Na_2SO_4 system. The Li_2SO_4-Na_2SO_4 system prove to be suitable for thermal energy storage primarily through solid-solid phase transition that occurs in a temperature range of 475-578 °C depending on the molar ratio between Li_2SO_4 and Na_2SO_4. In order to analyze this characteristic, and subsequently characterize the material mechanically, the ink development is crucial to simplify the production and ensure repeatability. Furthermore, additive manufacturing, as a forming method, expands the range of potential applications as it allows for the creation of complex and customizable designs that can accommodate volume changes during the solid-solid phase transition. The Direct-Ink-Writing technique is a technology that allows 3D printing of the ink starting from a solution of salts, a binder, and a solvent. To produce the ink, the salts are first ground and sieved to achieve dimensional uniformity. A binder, PVP (Polyvinylpyrrolidone), and ethanol, as a solvent, are then added.

I due sali sono Li_2SO_4 e Na_2SO_4. Sono due sali ternari che, se usati insieme, creano il sistema Li_2SO_4-Na_2SO_4. Il sistema Li_2SO_4-Na_2SO_4 si è rivelato adatto all'accumulo di energia termica soprattutto grazie alla transizione di fase solido-solido che si verifica in un intervallo di temperatura compreso tra 475 e 578 °C a seconda del rapporto molare tra Li_2SO_4 e Na_2SO_4. Per analizzare questa caratteristica, e successivamente caratterizzare il materiale dal punto di vista meccanico, lo sviluppo dell'inchiostro è fondamentale per semplificare la produzione e garantire la ripetibilità. Inoltre la fabbricazione additiva, in quanto metodo di formatura, amplia la gamma di potenziali applicazioni in quanto consente la creazione di modelli complessi e personalizzabili, in grado di adattarsi alle variazioni di volume durante la transizione di fase solido-solido. La tecnica Direct-Ink-Writing è una tecnologia che permette di stampare in 3D l'inchiostro partendo da una soluzione di sali, un legante e un solvente. Per produrre l'inchiostro, i sali vengono prima macinati e setacciati per ottenere l'uniformità dimensionale. Vengono poi aggiunti un legante, il PVP (Polivinilpirrolidone), e l'etanolo, come solvente.

Contents

Contents

List of Figures

1 Introduction

1.1 Phase change materials

Phase change materials (PCM) are an alternative to build compact, simple and low-cost thermal energy storage due to the necessity to decarbonize our society and promote the development of renewable energy sources [5]. This type of material is used, in particular, with renewable energy like solar and wind, offering good thermal energy storage via the enthalpy change of a phase transition that could be melting or solid solid transition. When a PCM is heated to its transition temperature, it undergoes a conversion from one phase to another. If the phase transition is a first-order process, it happens at a constant temperature and requires an input of energy at the transition temperature. This energy input is known as the transition enthalpy change or latent heat. If the phase change is reversible, the stored energy can be recovered through cooling [13]. Additionally, any energy input required to heat the PCM to its transition temperature and any energy input to further raise its temperature after the phase transition are stored as sensible heat. Therefore, the PCM can store a total quantity of heat over the temperature range T_1 to T_2 [13]:

$$Q = \int_{T_{trs}}^{T_1} mc_{p,1}(T)dT + m\Delta_{trs}H + \int_{T_2}^{T_{trs}} mc_{p,1}(T)dT \qquad (1.1)$$

where T_{trs} is the transition temperature, $\Delta_{trs}H$ is the transition enthalpy change, $c_p, 1$ is the specific heat capacity of the low-temperature phase, and $c_p, 2$ is the specific heat capacity of the high-temperature phase. PCMs absorb heat when the temperature is
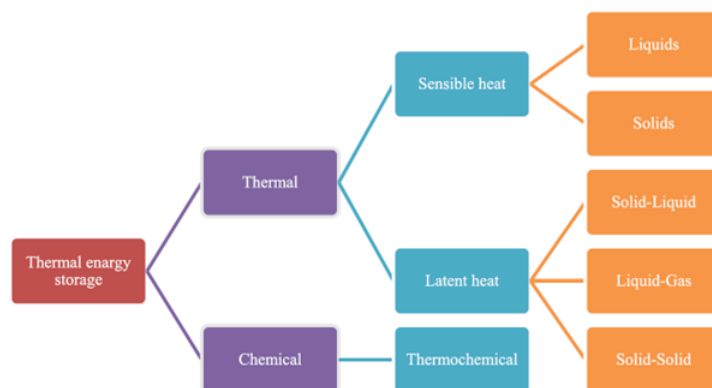
Figure 1.1: *Classification of TES material [5]*

high and release its stored energy when the temperature has dropped, maintaining the

1

temperature in the environment mild, avoiding peak of extreme high or extreme low temperature. The PCMs has to undergo its phase transition within the range of temperature of its application because otherwise the enthalphy change of phase transition is not accessed, and much of the thermal storage capacity is lost. There are other important properties to consider for a working PCM: thermal conductivity, heat capacity, stability, cyclability, phase segregation, supercooling, containment, cost and safety [13]. Thermal conductivity measures the heat conduction in a material. Insufficient thermal conductivity will impede the efficient charging and timely extraction of energy from the PCM. High heat capacity, instead, will maximize the amount of sensible heat the PCM can store in addition to its latent heat storage [13]. Phase change materials find applications in various fields, such as building construction, energy storage, and electronics cooling. In buildings, in fact, them can be integrated into walls, ceilings, or floors to regulate indoor temperatures by absorbing excess heat during the day and releasing it at night when temperatures drop. This helps in reducing the need for mechanical heating or cooling systems, leading to energy savings. Additionally, PCMs, are utilized in electronics cooling applications to absorb and dissipate heat generated. They can enhance the thermal management of electronic components and prevent overheating, prolonging the lifespan and improving the efficiency of electronic devices. Overall, phase change materials provide an efficient and sustainable solution for thermal energy storage and management.

1.2 Additive Manufacturing

In 1987, the invention of stereolithography marked the birth of additive manufacturing (AM). This quickly emerging manufacturing technology utilizes computer-aided design (CAD) information to construct parts in a layer-by-layer fashion. AM has revolutionized manufacturing by allowing the production of intricate shapes, reducing manufacturing costs, and minimizing energy consumption. It has shifted the manufacturing paradigm from mass production to mass customization. Despite a few drawbacks, AM has found extensive applications across various industries. Additive manufacturing 3D printing, is a process of creating three-dimensional objects by adding materials layer by layer based on a digital design. Unlike traditional manufacturing methods that involve subtracting materials or shaping objects through molds, additive manufacturing builds up objects by depositing materials. Commonly the materials used are plastic, metal and ceramics. The growing agreement of adapting the 3D manufacturing system over traditional techniques is attributed to several advantages [12]:

- Fabrication of complex geometry

- High precision

- Material saving

- Flexibility in design and personal customisation

- Topological optimisation

- Fabrication of parts of various sizes from the micro-to macro-scale

- Near net shape component

On the other hand, AM shows some limitations which lead to many challenges in developing production processes [12]:

- Anisotropic behaviour

- Inferior mechanical properties

- Void formation

- Printing environment influences the quality of finished products and the printing phase

- Difference between CAD model and the printed object

- Limited selection of suitable materials

- Precision is strictly linked to the accuracy of the technology used

- Issues with resolution, layered appearance and layer bonding

- Time consuming and Expensive process that are an obstacle for mass production
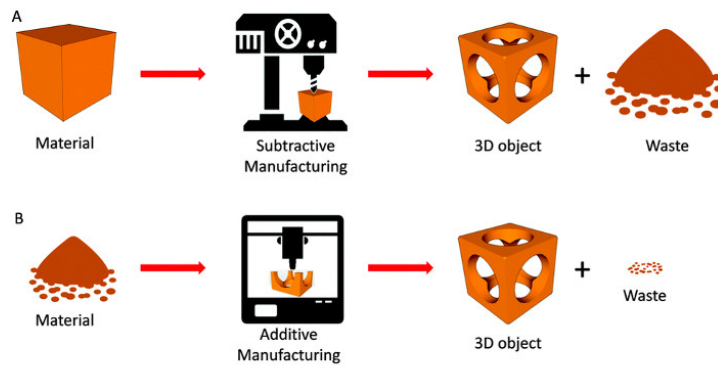
Figure 1.2: *(A) Subtractive manufacturing, (B) Additive manufacturing*

1.2.1 Direct ink writing

One of the most widely used and practical techniques is extrusion-based additive manufacturing (AM) using direct ink writing. DIW, which stands for Direct Ink Writing, is an additive manufacturing technique that allows for the creation of complex and detailed 3D structures at the micro and mesoscale. This method involves the extrusion of a viscoelastic ink material through a deposition nozzle in a layer-by-layer fashion. The ink is carefully controlled and deposited onto a movable stage, following a pre-determined computer-generated design. Once the ink is extruded, it solidifies, resulting in the formation of a 3D structure with specific desired features and properties. This process is commonly referred to as Robocasting as well. There are two main categories that DIW
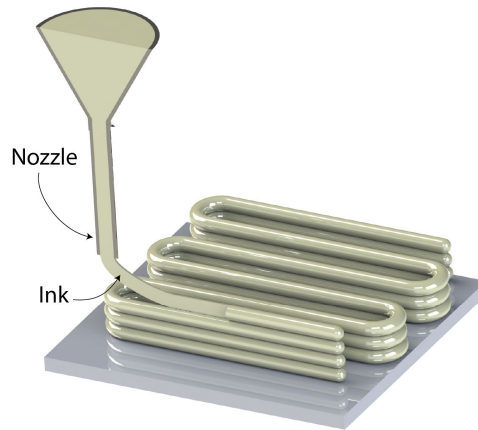
Figure 1.3: *Ink deposition [1]*

can be divided into: droplet and continuous ink extrusion. In droplet-based DIW, the ink is dispensed in small droplets, which are carefully placed and arranged to form the desired structure. This method allows precise control of ink placement with the ability to create complex geometries. On the other hand, continuous ink extrusion involves the extrusion of a continuous stream of ink material. This method is more suitable for creating structures with larger dimensions and simpler geometries, as it does not allow for the same level of detail as droplet-based DIW. Overall, DIW, provides a versatile and efficient way to fabricate complex 3D structures with varying compositions and architectures [16]. In all material extrusion-based technologies, pressure is applied to force the material out through a nozzle from a tank. When the pressure remains constant, the extruded material flows at a consistent rate and maintains a constant cross-sectional diameter. To achieve this, it is necessary to keep the speed of the nozzle's movement across the surface at a constant rate corresponding to the flow rate. The material being extruded should be in a semi-solid state when exiting the nozzle and solidify completely while retaining its shape. Additionally, it must bond with previously extruded material to form a solid structure [8]. There are two main approaches to the extrusion process. The most commonly used is to control the state of the material through temperature by increasing or decreasing its viscosity depending on the temperature set in the printing chamber, alternatively, a physical-chemical change can be used to induce solidification.

In other cases, curing can take place through the use of a curing agent, a residual solvent that will then be removed, e.g. through evaporation, reaction with air or drying of a wet material. The parts must polymerise or dry to achieve full stability. This approach is suitable for paste materials. By adjusting printer parameters such as pressure and speed, the printing process can be controlled to achieve the desired result. DIW technology has the added benefit of minimal post-processing and reduction in material waste, thus making the overall manufacturing process more economical and sustainable [16].

2 Materials

2.1 Li$_2$SO$_4$

Li$_2$SO$_4$ (lithium sulfate) is an inorganic compound composed of two lithium ions (Li$^+$) and one sulfate ion (SO$_4^{2-}$). It is a white crystalline powder, soluble in water and slightly
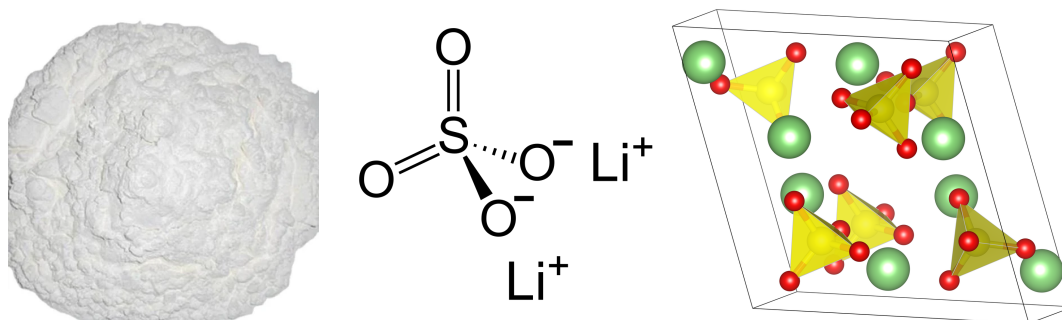
Figure 2.1: *Li$_2$SO$_4$ powder, structure Li$_2$SO$_4$,* ▮ *Li$^+$,* ▮ *S^{6+},* ▮ *O^{2-}*
[18]

soluble in alcohol. Lithium sulfate is commonly used in the production of rechargeable lithium-ion batteries due to its ability to function as an electrolyte meaning it can conduct electricity when dissolved in water. It is also utilized in various industrial applications, such as in the manufacturing of ceramics, glass, and detergents. The compound has a molar mass of approximately 109.94 grams per mole. It has a melting point of around 860 °C and does not undergo significant decomposition upon heating. Lithium sulfate has two different crystal phases: a common phase II and phase I. In phase II, Lithium sulfate has a sphenoidal monoclinic crystal system that has edge lengths of a=8.23Å, b=4.95Å, c=8.47Å, β=107.98°. When it is heated over 130 °C it changes to a water free state but retains its crystal structure. It is not until 575 °C when there is a transformation from phase II to phase I. The crystal structure changes to a face centered cubic crystal system, with an edge length of 7.07Å. [14].

2.2 Na$_2$SO$_4$

Na$_2$SO$_4$, or sodium sulfate, is an inorganic compound, with rhombohedral crystalline form, that appears as a white crystalline powder or a solid. It is composed of two sodium ions (Na$^+$) and one sulfate ion (SO$_4{}^{2-}$). It is highly soluble in water and and

Figure 2.2: *Na₂SO₄ powder, structure Na₂SO₄ [19]*

insoluble in alcohol. This salt is commonly used in various industries, such as detergents, glass manufacturing, and the production of paper and textiles. It is also used in water treatment processes to remove calcium and magnesium ions, as well as in the preparation of other chemicals. Also This compound is an electrolyte like Li_2SO_4. It can form hydrates, with the most commonly encountered being sodium sulfate decahydrate ($Na_2SO_4 \cdot 10H_2O$) also called Glauber's salt. Anhydrous sodium sulfate exists in a number of different polymorphous forms commonly referred to as phases I–V. Phases I, II and IV are high-temperature forms while metastable phase III can be kept indefinitely under dry conditions at room temperature, it is readily transformed into $Na_2SO_4(V)$ at enhanced relative humidity [19]. Na_2SO_4 is not considered toxic, but it can cause irritation to the skin, eyes, and respiratory system if it is inhaled or comes into contact with these areas.

2.3 Li_2SO_4-Na_2SO_4

Li_2SO_4-Na_2SO_4 is a very promising system for solid-state thermal energy storage applications due to its exceptional ionic conduction properties and this is why is used in the manufacture of batteries, in particular as a component in the cathode material. The stoichiometric compound $LiNaSO_4$ (lithium sodium sulphate) within this system is particularly noteworthy, as it acts as an established superionic conductor. At temperatures above 515 °C, $LiNaSO_4$, exhibits a remarkable characteristic known as quasi-liquid cationic sub-lattice. This means that the cationic sites within the crystal structure of $LiNaSO_4$ behave as if they were in a liquid-like state, resulting in increased ion mobility and conduction [6]. It undergoes a first-order phase transition where the high-temperature cubic phase exhibits high cationic conductivity and cation mobility is enhanced by a strong coupling with the rotation of the translocated sulphate ions [7]. The kinetics of the phase transition is mainly governed by cation diffusion.

This study examines four compositions of the Li_2SO_4-Na_2SO_4 system, namely: 100/0, 79/21, 50/50 and 0/100 (molar ratio), as potential materials for thermal energy storage at high temperatures (450-550 °C). The 79/21 and 50/50 compositions correspond to two important points in the theoretical phase diagram: an eutectoid and a solid-solid phase transition, and it is these two compositions that will play a role as PCMs. The other two compositions were made to evaluate the chemical and structural evolutions of the two starting salts during printing and during heat treatment. An important aspect

of a phase change material is the high transition enthalpy, so that it can store more heat during the phase transition that occurs at that constant T. The compatibility of this salt system with air is equally important: it allows its processing, and thus the realisation of structured components, and its handling then, easier because no inert environment is required. This aspect is also important for the utilisation phase: the component can be used as a normal heat sink using just air as the cooling fluid, cutting costs. To summarise: the Li_2SO_2-Na_2SO_4 system has potential as a system for thermal energy storage applications due to its high phase transition enthalpy, compatibility with air and making it easier to realise and use, and the solid-state nature of the components.
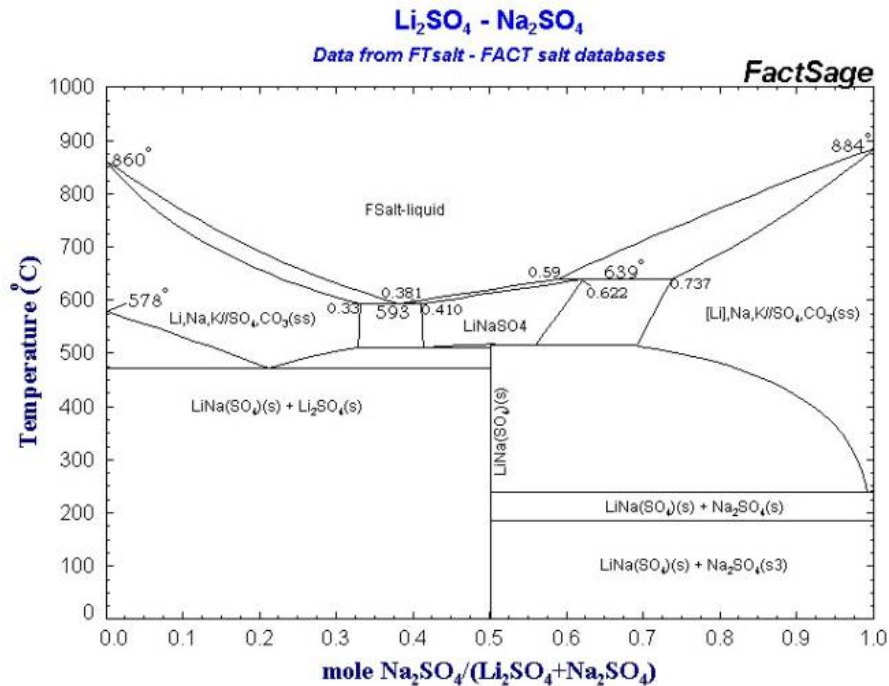
Figure 2.3: *The theoretical phase diagram [6]*

2.4 Polyvinylpyrrolidone (PVP)

Polyvinylpyrrolidone is a synthetic polymer made from the monomer N-vinylpyrrolidone. It is a white, amorphous powder that is highly soluble in water and other polar solvents. PVP is commonly used in various industries, including pharmaceuticals, cosmetics, and food processing.

One of the main characteristics of PVP is its ability to form stable complexes with other molecules. It acts as a binder, film-former, and stabilizer in many applications. In the pharmaceutical industry, PVP is used as a component in tablet coatings, where it improves the appearance, durability, and disintegration qualities of the tablets. It is also a common ingredient in suspensions, ointments, and eye drops. PVP is widely used in the cosmetics industry as a thickening agent, emulsifier, and stabilizer. It is found in
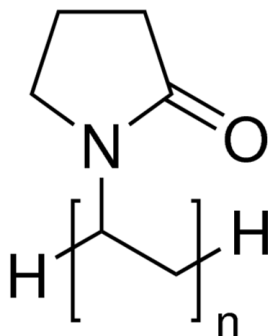
Figure 2.4: *Structure of Polyvinylpyrrolidone*

various personal care products such as hairsprays, shampoos, lotions, and creams. Its water solubility makes it easy to incorporate into formulations and provides a smooth and glossy finish. PVP is also known to enhance the stability and spreadability of cosmetic products. Another application of PVP is in the food industry, where it is used as a clarifying agent, emulsifier, and stabilizer. It helps to prevent the formation of crystals in food products and enhances their texture and appearance.

Overall, Polyvinylpyrrolidone is a versatile polymer that offers various benefits, including solubility, stability, film-forming properties, and compatibility with other ingredients. Its widespread use in different industries highlights its importance as a functional additive in many products.

2.5 Ethanol absolute

Ethanol absolute is a highly concentrated form of ethanol. It is a colorless liquid. It is produced through a process called rectification, which involves purifying ethanol to remove impurities and water. As a result, ethanol absolute has a purity of 99.9% or higher, has a chemical formula of C_2H_5OH, is highly flammable and evaporates quickly. It is miscible with water, meaning it can be easily mixed in any proportion with water. It is commonly used as a fuel additive to enhance the octane level of gasoline and improve combustion efficiency. Due to its antiseptic properties, ethanol is also employed as a disinfectant and sterilizing agent in medical and laboratory environments.

It was chosen to use ethanol and not water because salts, being hygroscopy, would tend to absorb water, causing phase separation not allowing the making of an ink . PVP was chosen for this study because it is soluble in the selected solvent (ethanol). After adding the salts, it will act as a binder for synthesising the ink.

3 Methods

3.1 Salts preparation

The main constituents of the ink are: Li_2SO_4, Na_2SO_4, ethanol and Polyvinylpyrrolidone. To be noted the anhydrous Li_2SO_4 and Na_2SO_4 powders must remain in contact with the atmosphere as little time as possible to avoid spontaneous hydration of the salts. The salts are milled to obtain a printable powder. During the milling phase there is a reaction in the solid state and this is confirmed by the partial conversion of the reactant in the phase $LiNaSO_4$.

Work was carried out with batches of 40 g, the material is placed in an agate ball milling jar which is shown in Fig. 3.1. The material is milled at 330 rpm for 10 rounds of 10 minutes each. The resulting powder is then sieved with a 63 micron mesh and stored in hermetically sealed containers. The two salts are then mixed in the correct stoichiometric ratio to then prepare the ink that will be printed (Li_2SO_4/Na_2SO_4 100/0, 79/21, 50/50 and 0/100) [6].

Figure 3.1: *Agate milling jar*

3.2 Ink preparation

The four components of the ink are:

- Lithium sulfate,for analysis, anhydrous (thermo scientific)

- Sodium sulfate, ACS, 99.0% min (thermo scientific)

- Polyvinylpyrrolidone (Sigma-Aldrich)

- Ethanol absolute, foranalysis, xpertQ, ACS, ISO (Scharlab)

Chemicals	MW (g/mol)	Density (g/cm^3)	Formula
Lithium sulfate	109,94	2,22	Li_2SO_4
Sodium sulfate	142,04	2,66	Na_2SO_4
Polyvinylpyrrolidone	40000	1,20	$(C_6H_9NO)_x$
Ethanol absolute	46,07	0,79	C_2H_5OH

It was necessary to create four distinct mixtures to print the four composition that will be studied and analyzed. The compositions are reported in the tables below.

- Tabel 3.1 100/0 (mol) Li_2SO_4/Na_2SO_4

- Tabel 3.2 79/21 (mol) Li_2SO_4/Na_2SO_4

- Tabel 3.3 50/50 (mol) Li_2SO_4/Na_2SO_4

- Tabel 3.4 0/100 (mol) Li_2SO_4/Na_2SO_4

Reagents	Mass (g)	wt%
Lithium sulfate	10	76,92
Sodium sulfate	0	0
Polyvinylpyrrolidone	0,69	5,31
Ethanol absolute	2,31	17,77

Table 3.1

Reagents	Mass (g)	wt%
Lithium sulfate	8,74	57,36
Sodium sulfate	3	19,68
Polyvinylpyrrolidone	0,69	4,53
Ethanol absolute	2,81	18,43

Table 3.2

Reagents	Mass (g)	wt%
Lithium sulfate	4,64	34,12
Sodium sulfate	6	44,12
Polyvinylpyrrolidone	0,65	4,78
Ethanol absolute	2,31	16,98

Table 3.3

Reagents	Mass (g)	wt%
Lithium sulfate	0	0
Sodium sulfate	11,5	79,31
Polyvinylpyrrolidone	0,69	4,76
Ethanol absolute	2,31	15,93

Table 3.4

To make the ink, the two salts must first be weighed, respecting stoichiometric ratios, depending on the composition to be printed. They are then placed in a container, the PVP is then added and lastly the absolute ethanol so as to limit loss through evaporation. The container is then placed in an orbital mixer (THINKY ARE-250 Fig. 3.2) and is mixed at 2000 rpm for 4 minutes to obtain a homogeneous mixture, avoiding overheating the ink to prevent the evaporation of absolute ethyl alcohol, thus making the mixture either too viscous for printing or even risking almost instantaneous drying in the syringe. The ink ($\sim$10 grams) is then loaded into the syringe and extruded through a 0.58 mm nozzle. Na_2SO_4 facilitates printing because it contributes to a more predictable rheological behaviour of the ink during printing.

Figure 3.2: *Orbital mixer*

Previously the possibility of making ink using water and carboxymethylcellulose (CMC) as a binder was considered, but as the two salts are hygroscopic, the result was a phase

separation, i.e. separation of solid phase: salt and CMC, and liquid phase: water. It was therefore necessary to opt for a binder that did not require water, so it was decided to use PVP with absolute ethanol.

3.3 Printing

Printing is carried out with a Delta 2040 Turbo 2 printer (Fig. 3.3a). The ink, previously placed in the syringe, is pushed through the nozzle, which in this case has a size of 0.58mm, by compressed air. The pressure is regulated manually via a Digital Dispenser DC 300 Series pressure regulator (Fig. 3.3b).
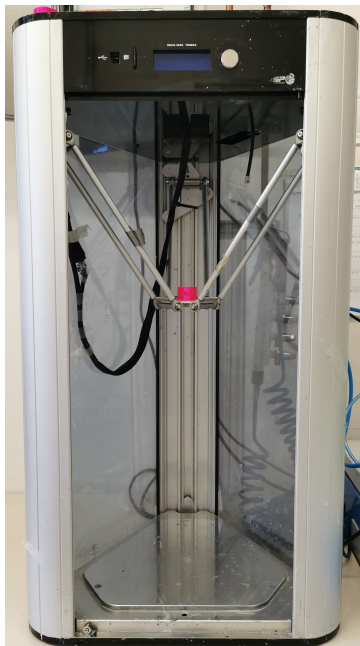
(a) *Printer*   **(b)** *Pressure regulator*

Figure 3.3: *Printing tools*

The filament is deposited continuously on a Polytetrafluoroethylene (PTFE) sheet, to facilitate detachment, layer upon layer until the final shape is achieved (Fig. 3.4a). During the process, as the ink is not very viscous to retain its shape, it is necessary to direct a jet of air directly onto it in order to accelerate the evaporation of the ethanol. These ink must be printed as soon as they are prepared (when the have low viscosity) at low pressures of about 0.2 bar. The printed specimen is cylindrical in shape with a nominal diameter of 14 mm and a nominal height of 5 mm. The print geometry is layered with an offset of 90 degrees (Fig. 3.4b). After printing, the samples are kept in air at room temperature for a week to fully dry the sample.
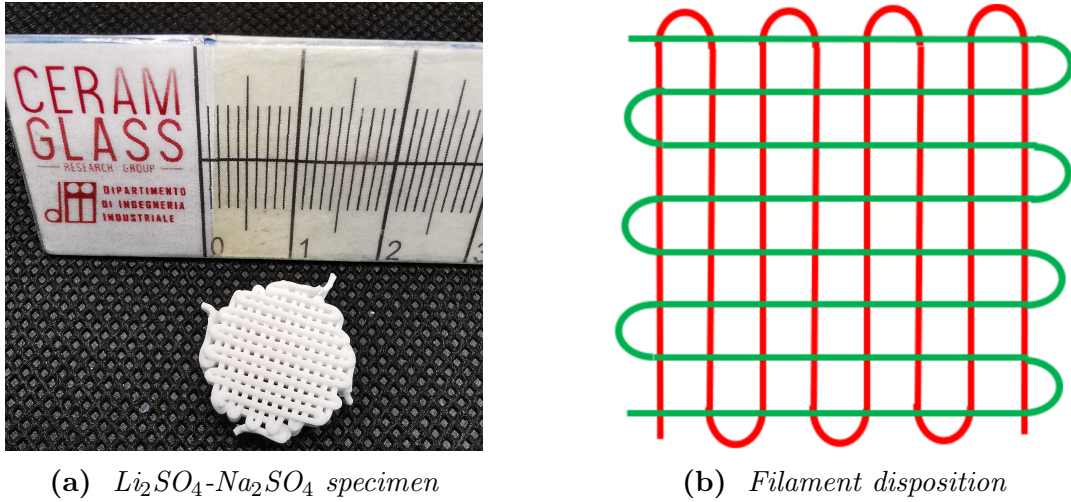
(a) *Li_2SO_4-Na_2SO_4 specimen*

(b) *Filament disposition*

Figure 3.4: *Printing method*

3.4 Thermal treatment

In the synthesis of the inks, it was necessary to add 4.53-5.31% PVP as a rheological additive to obtain a printable mixture. In order to achieve the greatest possible heat exchange during use, the printed components must have the lowest possible impurity content. Furthermore, polyvinylpyrrolidone can be removed without causing any deterioration in the structure. The objective of the thermal treatment is also to remove all water, present in the hydrated salts, which could compromise the phase change or the correct heat exchange between environment and sample.

A thermal cycle with T_{max} = 400 °C (Fig. 3.5a) was carried out as a first test and then, as a second test, one with T_{max} = 600 °C (Fig. 3.5c), in order to evaluate through XRD (X-ray diffraction) whether there are any changes in structure and phase. Another thermal cycle at T_{max} = 500 °C (Fig. 3.5b), instead of the cycle with T_{max} = 600 °C, was performed only on composition 50/50 (mol) Li_2SO_4/Na_2SO_4 in order to avoid reaching the eutectic (around T= 600 °C). The (Fig. 3.5a) heating cycle was performed in two steps: a first ramp to 300 °C at 1 °C/min, stationary temperature for 3 hours, followed by a second ramp to 400 °C at 1 °C/min, 1h dwell and slow cooling with the furnace off until room temperature. The other heating cycle (Fig. 3.5b) is a 3 step heating. First ramp to 300 °C at 1 °C/min, stationary temperature for 1 hours, a second ramp to 400 °C at 1 °C/min, 1h dwell and the third ramp to 500 °C at 1 °C/min and stationary temperature for 1 hour. Subsequentially, the cooling phase: the ramp chosen is the same. The ramp in Fig. 3.5c is the same as Fig. 3.5b with a higher T_{max}. An example of a pre and post heat treatment specimen can be seen in Fig. 3.6.

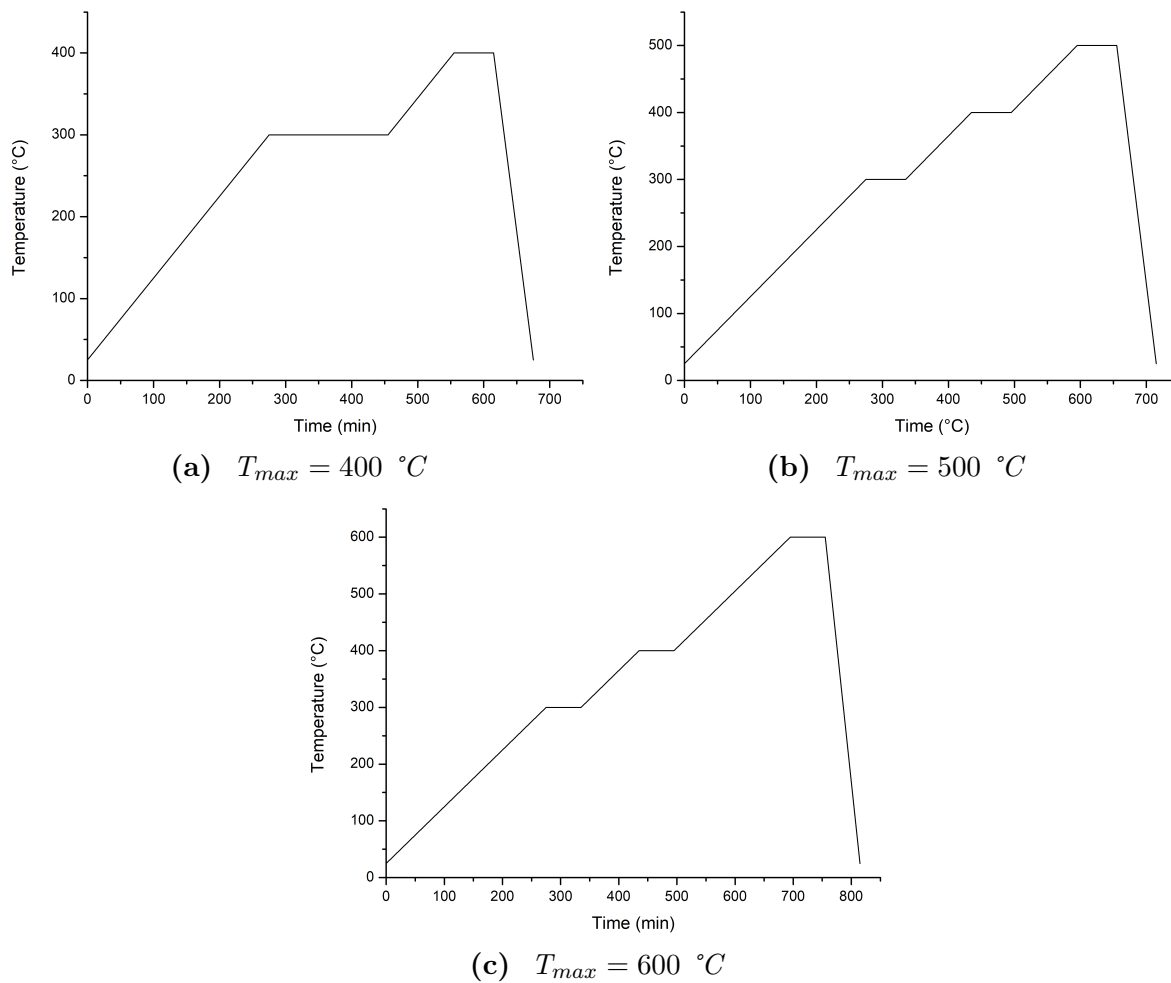**(a)** $T_{max} = 400$ ˚C

(b) $T_{max} = 500$ ˚C

(c) $T_{max} = 600$ ˚C

Figure 3.5: *The 3 different heating cycle*

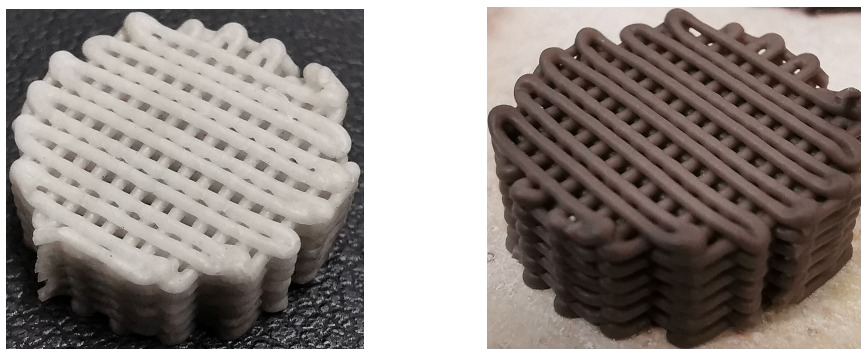**Figure 3.6:** *Sample 50/50 (mol) Li_2SO_4/Na_2SO_4, on the left pre heat treatment and on the right post heat treatment*

3.5 Mechanical properties

The fracture of brittle materials (in this case a ceramic material) usually starts from distributed defects in the material. The strength of the specimen depends on the size of the main defects, which vary from specimen to specimen. Therefore, the strength of brittle materials must be described by a statistical probability function. The Weibull distribution function is the basis of the state-of-the-art mechanical design procedure for ceramic components. The basic assumption is that the specimen breaks if its weakest volume element breaks. Experiments show that the probability of rupture increases with the magnitude of the load and the size of the specimen. Weibull is a statistical distribution that is commonly used to model reliability data and failure times. It was first introduced by Wallodi Weibull, a Swedish engineer and mathematician, in the 1950s. The crucial aspect of ceramic materials is their brittleness and the distribution of defects, which significantly contribute to the unpredictability of failure and undermine the reliability of experimental fracture data. This is why the most commonly used approach to describe the mechanical strength of a ceramic is the Weibull distribution. If the rupture results of a sufficient number of samples are plotted in a histogram, this graph can be described analytically by a function called the Weibull distribution density [9]:

$$f\left(\frac{\sigma}{\sigma_0}\right) = \frac{m}{\sigma_0}\left(\frac{\sigma}{\sigma_0}\right)^{m-1} \cdot exp\left[-\left(\frac{\sigma}{\sigma_0}\right)^m\right] \tag{3.1}$$

where m is the Weibull module, σ is the fracture stress, and σ_0 is a normalisation parameter. As the m-value increases, the distribution becomes narrower, which is expressed in a higher accuracy of the fracture data. The survival probability for a given σ value can instead be expressed in two ways [9]:

$$S = exp\left[-\left(\frac{\sigma}{\sigma_0}\right)^m\right] \tag{3.2}$$

$$\ln\ln\frac{1}{S} = m\ln\frac{\sigma}{\sigma_0} = m\ln\sigma - m\ln\sigma_0 \tag{3.3}$$

Reporting in a graph $\ln\ln(1/S)$ vs $\ln\sigma$ is it possible to extract, for experimental data, the value of m and σ_0 and then obtain S for each value of σ. To determine the values of m and sigma zero, it is necessary to plot the Weibull diagram for each batch. This can be done by ordering the fracture stress values of the N samples from smallest to largest. For each specimen, its corresponding survival probability S_j can be calculated using the following approximate relation [17]:

$$S_j = \frac{j-a}{N+b} \tag{3.4}$$

where a and b are two parameters, comprised between 0-1.0 and 0-0.5 respectively, whose value depends on N.

3.6 X-ray diffraction

X-ray diffraction is used to study the atomic and molecular structure of materials. This technique exploits the scattering at specific angles of x-rays due to their interaction with the crystalline substance being analysed. This scattering pattern shows important information about the arrangement of atoms in crystals.The working principle of X-ray diffraction revolves around the wave-particle duality of X-rays. When X-rays interact
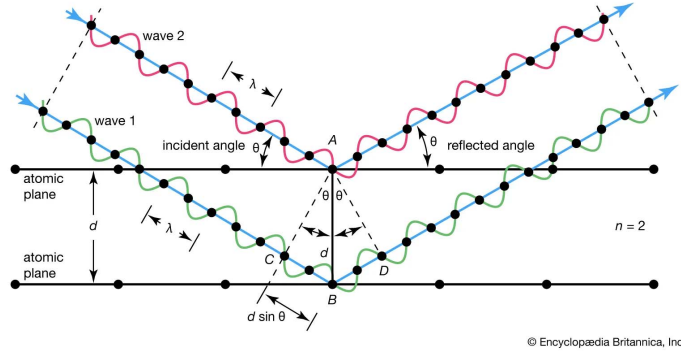

Figure 3.7: *Bragg diffraction*

with a crystal lattice, they behave like waves and undergo constructive and destructive interference. The scattering of X-rays occurs due to the interaction of the incident X-ray beam with the electrons of the crystal's atoms. To obtain a diffraction pattern, a sample is placed in the path of a monochromatic X-ray beam. The X-rays interact with the crystal lattice and scatter in various directions. However, constructive interference occurs when the scattered waves meet at specific angles, which are determined by the spacing between the crystal planes and the wavelength of the X-rays. The scattered X-rays are detected by a detector, such as a photographic film, a phosphor screen, or a digital detector. The resulting diffraction pattern is a series of spots or rings and the intensity and position of these spots provide information about the angles at which the X-rays were scattered and the distance between the crystal planes. These patterns are determined by Bragg's law. This law is defined as [10]:

$$n\lambda = 2 \cdot sin\theta \tag{3.5}$$

Parameter n is the order of diffraction, λ is the wavelength of the incident x-rays, d is inter-planar spacing involved and θ is the angle between the incident (or diffracted) ray and the relevant crystal planes. The use of peak indexing software (Match!) enables the comparison of measured XRD patterns with reference databases, facilitating the identification and approximate quantification of the phase of interest. All the samples were subjected to XRD measurements in the 5-70 θ range.

In this study, XRD was used to evaluate the atomic and molecular str uctural evolution of the specimens. Specimens were analysed after printing and after undergoing heat treatment in order to assess differences in composition.

3.7 Scanning electron microscopy SEM

Scanning electron microscopy (SEM) is a technique used to observe the surface features of a sample at high resolution. Quanta 200 was used in this study (Fig. 3.8). It

Figure 3.8: *SEM*

provides detailed information about the morphology, topography and composition of a sample. A high-energy point beam of electrons, generally between 0.1-30 keV, called the primary beam, is generated by heating a tungsten and focused on the surface of the system under test under vacuum conditions to avoid interference of the beam with atmospheric dust. This beam of primary electrons interacts with the atoms on the surface of the sample, causing various signal emissions. These emitted signals include secondary electrons, backscattered electrons and X-rays. Secondary electrons are the most commonly used signal in SEM. They are the result of the inelastic collision and scattering of incident electrons with specimen electrons. They have a low energy and are emitted from the upper few nanometres of the sample surface. Backscattered electrons, on the other hand, have a higher energy and are emitted from deeper within the sample due to scattering events between incident electrons and nuclei in the analysed sample, providing information on its composition. The emitted electrons are collected by detectors and converted into electrical signals. These signals are then amplified, processed and displayed on a screen, forming an image of the sample surface. The image is created by scanning the electron beam through the sample in a raster pattern and measuring the signal intensity at each point. The SEM provides high-resolution images with magnifications from 10x to over 4000x, depending on the instrument and sample characteristics. It also allows elemental composition to be analysed using energy dispersive X-ray spectroscopy (EDS), which measures the characteristic X-rays emitted by the sample. EDS works by bombarding the sample with a focused beam of high-energy electrons, which causes the atoms in the sample to emit characteristic X-rays. These X-rays are then detected by an EDS detector and analyzed to determine the identity and quantity of

the elements present. The detector used in EDS consists of a solid-state semiconductor crystal, such as silicon, which generates a small electrical pulse each time it absorbs an X-ray photon. The energy of each pulse is directly proportional to the energy of the X-ray photon that caused it. The collected X-rays are sorted according to their energy using an energy-dispersive spectrometer, which consists of a crystal and a detector [3]. The crystal disperses the X-rays, separating them based on their energy and directing them towards the detector. The detector then measures the energy of the X-rays, generating a spectrum that shows the distribution of different elements in the sample. The EDS spectrum is typically displayed as a graph, with the energy of the X-rays plotted on the x-axis and the number of X-rays detected at each energy plotted on the y-axis. Peaks in the spectrum correspond to specific elements present in the sample, and the height of each peak indicates the abundance of the corresponding element. In addition to imaging, SEM can be used for various applications, including microstructural analysis, quality control, failure analysis, forensic investigation and biological research. In general, scanning electron microscopy provides a powerful tool for examining the surface characteristics of materials and obtaining valuable information on their structure and composition.

3.8 Differential scanning calorimetry DSC and Thermogravimetric analysis TGA

Differential scanning calorimetry is a thermal analysis technique used to measure how a material's heat capacity (C_p) is changed by temperature. It is used to study thermal properties, estimate the purity of a material, as well as its stability and the presence of polymorphisms. In a DSC analysis, the sample and reference material are subjected to a controlled temperature programme in which the temperature is gradually increased or decreased. As the temperature changes, the heat flow required to maintain the sample and reference at the same temperature is measured. Any difference in heat flow between the sample and the reference is recorded as a signal highlighting the thermal events occurring in the sample material. The device used in this work is the Thermal Analysis System TGA/DSC 3+ (Fig. 4.23). For example, if the sample undergoes a phase transition, such as melting or crystallization, there will be a heat flow change that is observed as a peak or a change in the baseline of the DSC signal. This allows to determine the specific temperature range and enthalpy associated with phase transitions. Thermogravimetric analysis (TGA), instead, is a technique used to study the thermal stability and composition of materials. It measures the change in mass of a sample as it is subjected to controlled heating or cooling in a controlled environment. During the analysis, the temperature of the furnace is gradually increased or decreased at a constant rate. As the temperature changes, various thermal events can occur, such as evaporation of volatile components, decomposition, or phase transitions. These events cause a change in the mass of the sample, weight loss normally occurs, which is detected by the balance providing information from which it is possible to draw conclusions regarding the thermal

Figure 3.9: *TGA/DSC*

properties and composition of materials.

In this study, the TGA was used to assess at what temperature PVP degradation was taking place so that the heat treatment temperatures could be set in the correct way to burn off all the binder.

3.9 Rheology

Rheology is defined as the study of the flow of matter, generally accounting for the behaviour of non-Newtonian fluids (their viscosity is dependent on shear rate) [15]. This science helps to understand how materials deform or flow when subjected to a stress, or strain, is applicable to a wide range of materials and in the field of materials science it plays an important role in the characterisation of materials. By studying the flow and deformation properties of different substances, it is possible to derive their structural properties in order to design then with specific properties such as stability, flexibility and viscosity. Various techniques and instruments are used to study rheology; in this thesis work, the Netzsch Kinexus Prime lab+ (Fig. 3.10) was used.

Figure 3.10: *Netzsch Kinexus Prime lab+*

Rheometers, which apply controlled stresses or deformations to a sample, are commonly used to measure viscosity, viscoelastic behaviour and other rheological properties. These measurements are usually obtained by subjecting the material to oscillatory, rotational or shear forces. Overall, rheology provides valuable information on how materials flow and deform, allowing their behaviour to be better understood, manipulated and optimised. It plays a critical role in fields where the flow and deformation properties of materials are crucial for their performance and functionality.

Viscosity is the manifestation of friction phenomena in the flow motion of fluids. Referring to Figure 3.11, consider a fluid layer of thickness L confined between two parallel flat parallel flat plates, if one of the two plates is set in motion with velocity v_0 in the direction and direction of x increasing, the fluid is dragged along with it and, at steady state, we will have a distribution of velocities in the fluid [11]. In addition to fluid
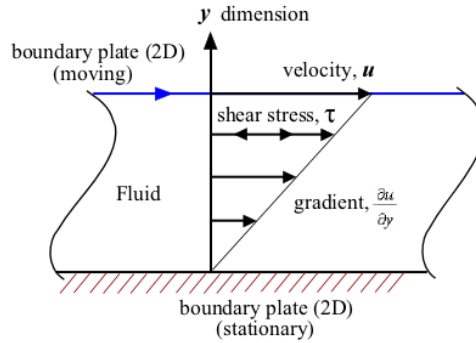

Figure 3.11: *Laminar motion between two walls [11]*

temperature, there may be other variables to consider when studying fluid behaviour. The type of fluid, whether it is dilatant viscous, Newtonian, or pseudoplastic, will determine how it behaves under shear stress. Shear stress can occur during processes such as mixing, pumping or flow through pipes. A pseudoplastic fluid, reacts differently when it comes into contact with a blade or shear stress, unlike other fluids, its viscosity decreases as it is pumped, transported, dosed, or atomized. The mechanisms responsible for pseudoplastic flow are due to the fact that these substances are not homogeneous, but consist of irregularly shaped particles dispersed in a liquid base, emulsions or molecules characterised by long chains. On the other hand, fluids such as water and cooking oil behave Newtonian, i.e. regardless of shear effects, they tend to maintain their viscosity. A dilatant, on the other hand, is a non-Newtonian fluid in which the shear viscosity increases with the applied shear stress. An example of this type of fluid is a mixture of cornstarch and water. This behaviour is typically observed in suspensions containing a substantial amount of solid particles that are not clumped together. When at rest, the spaces between the suspended particles are minimized, allowing for a limited flow of the fluid permeating those spaces. However, as the applied stress intensifies, the particles start to move and collide with each other. This collision leads to an enlargement of the free spaces between the particles, which cannot be filled by the liquid vehicle. As a result, the liquid is unable to provide sufficient lubrication.
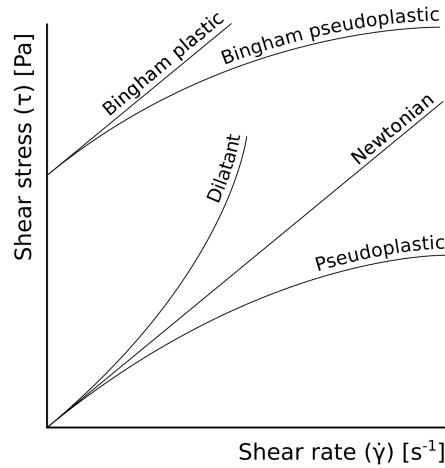
Figure 3.12: *Classification of fluids with shear stress as a function of shear rate [4]*

3.10 Density

Helium pycnometry aims to find volume and true density using Archimedes' fluid over-flow principle and Boyle's Law. For maximum accuracy of measurements, the overflowing fluid must be an inert gas that can enter all but the smallest pores. Therefore, Helium gas with small atomic dimensions approaching recesses and pores with a diameter of 0.25 nm is considered suitable for measurements. Helium's behaviour as an ideal gas is also a reason for preference. Even when other gases are used (such as nitrogen), there is usually no measurable difference. For structures with helium permeability (such as low-density polymers and plant-derived materials), nitrogen or SF6 gas must be used [2]. Two measurements were carried out to calculate the density of the samples. The first was made on the powdered specimens in order to calculate the actual density of the printed ink, the second measurement was made on whole pieces of lattice, in order to calculate the density of the printed specimens. A lower density is expected when measuring the lattices as closed porosity is also present.

Figure 3.13: *Anton Paar Ultrapyc 3000*

4 Results

4.1 Mechanical performances

As seen theoretically in section 3.5, the Weibull model is used to evaluate mechanical performance under compression. In ceramic materials, being brittle materials, in order to measure the reliability and probability of failure, it is important to calculate the Weibull modulus m, which can be derived from mechanical compression test data. The mechanical properties of this type of material are negatively affected by the presence and distribution of micro-cracks and surface defects, which is why the statistical approach is used. Tables 4.2, 4.3, 4.4 show data on dimensions, stress at break and probability of survival for each composition tested. 10 specimens were tested for each of the 3 compositions considered most interesting on a theoretical level. The specimens were all heat-treated before the mechanical tests. Compression test results in terms of Weibull Parameters, the number of specimens tested N and the parameters a and b are reported in table 4.1.

Specimen	N	m	σ_r (MPa)	a	b
100/0 (mol) Li_2SO_4/Na_2SO_4	10	2,52	5,33	0,5	0.00
79/21 (mol) Li_2SO_4/Na_2SO_4	10	2,23	8,80	0,5	0.00
50/50 (mol) Li_2SO_4/Na_2SO_4	10	1,27	8,43	0,5	0,00

Table 4.1

The values of σ at break, for each group of samples, were highly variable despite the fact that the composition and print geometry were the same. This dispersion of values can be explained by the unpredictability and variety of defects like filament positioning, presence of air bubbles, or heat treatment-induced cracks. Weibull modulus values (value m in Table 4.1) for the 3 compositions were low compared to values of ceramic materials, that are above 5 up to about 20. The survival analysis makes it clear that the survival probability of the sample that yielded to the lower load is obviously the highest. Take Tab. 4.2 as an example: it can be seen that scrolling down the list of samples, being ordered according to the increase of the stress at break, as the breaking load increases, the probability of survival decreases and, consequently, the probability of failure increased [9]. The survival probability can be calculated using the formula 4.2. With these results, the following statements can be done:

- 100/0 (mol) Li_2SO_4/Na_2SO_4: internal filament's structure is shown in Fig. 4.12.

This batch of samples has the largest Weibull modulus (m=2,52), which normally means that the defects are more similar.

- 79/21 (mol) Li_2SO_4/Na_2SO_4: internal filament's structure is shown in Fig. 4.15. This lot has a Weibull modulus close in value to that of Li_2SO_4 but still lower due to the presence of Na_2SO_4, which worsen the survival distribution. This can also be seen from the scattering of values in the results. These specimens presented high value of both maximum compressive strength (8,43 MPa) and minimum strength (1,93 MPa).

- 50/50 (mol) Li_2SO_4/Na_2SO_4: internal filament's structure is shown in Fig. 4.20. This batch has the lowest Weibull modulus (m=1,27), of the 3 different compositions, this is the one that contains the most Na_2SO_4 and looking at the filament section it is the one with the densest and largest porosity and cracks. There is a lower minimum stress at fracture (0,53 MPa) and a higher maximum stress at fracture (8,53 MPa), marking a greater dispersion of strength values.

The fact that by increasing the concentration of Na_2SO_4 the mechanical properties decrease may indicate that by increasing the concentration of $LiNaSO_4$ in the treated samples, the Weibull modulus decreases. This means that the values at fracture will be more distributed and it will be more difficult to predict the failure of the structure due to its brittle behaviour.
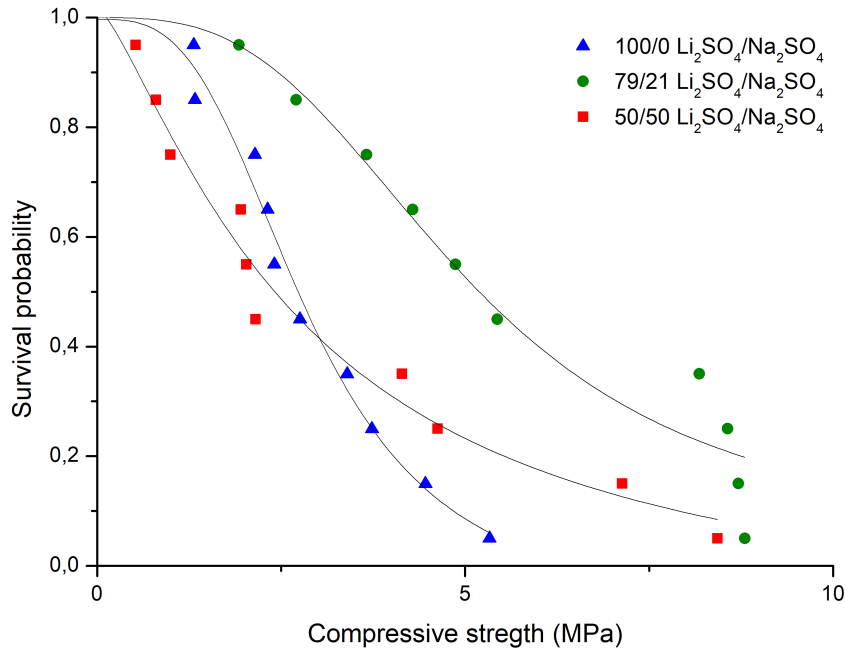

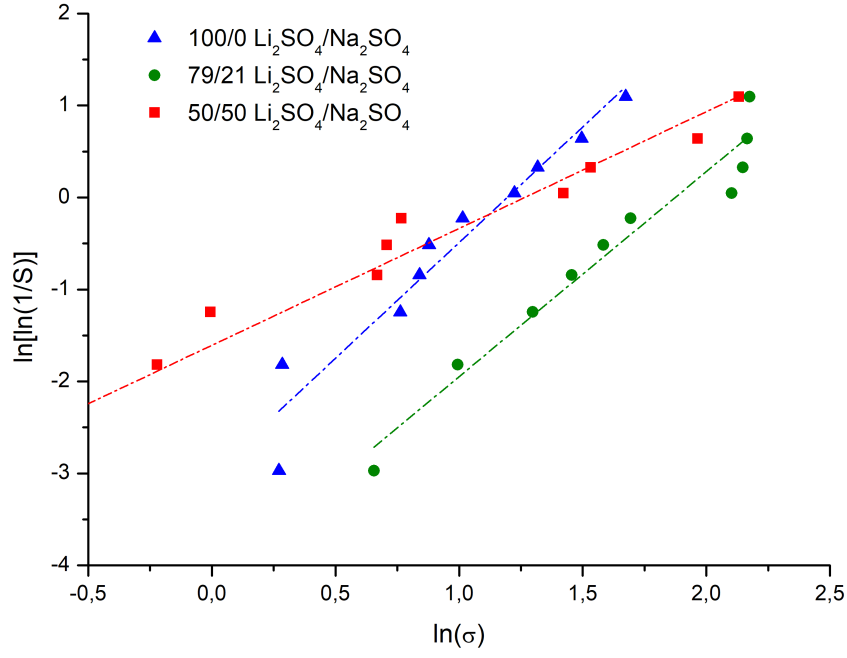**Figure 4.1:** *Rupture data fitting according to Weibull model in exponential form*

Figure 4.2: *Rupture data fitting according to Weibull model in exponential form*

j	D (mm)	h (mm)	A (mm^2)	σ	S	ln σ	lnln(1/S)
1	13,35	4,76	139,91	1,31	0,95	0,27	-2,97
2	13,41	4,72	141,17	1,33	0,85	0,28	-1,82
3	13,20	4,73	136,78	2,14	0,75	0,76	-1,25
4	13,40	4,65	140,95	2,32	0,65	0,84	-0,84
5	13,25	4,73	137,82	2,41	0,55	0,88	-0,51
6	13,06	4,38	133,89	2,76	0,45	1,01	-0,23
7	13,21	4,58	136,99	3,40	0,35	1,22	0,05
8	13,46	4,94	142,22	3,74	0,25	1,32	0,33
9	13,31	4,22	139,07	4,46	0,15	1,50	0,64
10	13,46	4,24	142,22	5,33	0,05	1,67	1,10

Table 4.2: *100/0 (mol) Li_2SO_4/Na_2SO_4*

j	D (mm)	h (mm)	A (mm^2)	σ	S	ln σ	lnln(1/S)
1	13,70	5,02	147,34	1,93	0,95	0,66	-2,97
2	13,65	4,70	146,26	2,71	0,85	0,99	-1,82
3	13,71	5,04	147,55	3,66	0,75	1,38	-1,25
4	13,71	4,91	147,55	4,29	0,65	1,46	-0,84
5	13,45	4,70	142,01	4,87	0,55	1,58	-0,51
6	13,82	4,92	149,93	5,44	0,45	1,69	-0,23
7	13,59	4,87	144,98	8,18	0,35	2,10	0,05
8	13,79	4,80	149,28	8,57	0,25	2,15	0,33
9	13,92	4,83	152,11	8,72	0,15	2,17	0,64
10	13,67	4,75	146,69	8,80	0,05	2,18	1,10

Table 4.3: *79/21 (mol) Li_2SO_4/Na_2SO_4*

j	D (mm)	h (mm)	A (mm^2)	σ	S	ln σ	lnln(1/S)
1	13,12	4,37	135,13	0,53	0,95	-0,64	-2,97
2	13,24	4,78	137,61	0,80	0,85	-0,22	-1,82
3	13,17	4,49	136,16	0,99	0,75	-0,01	-1,25
4	13,18	4,64	136,36	1,95	0,65	0,67	-0,84
5	13,41	4,72	141,17	2,03	0,55	0,71	-0,51
6	14,73	4,99	170,32	2,15	0,45	0,77	-0,23
7	13,25	4,58	137,82	4,14	0,35	1,42	0,05
8	13,23	4,46	137,40	4,63	0,25	1,53	0,33
9	13,55	4,77	144,13	7,14	0,15	1,97	0,64
10	13,38	4,66	140,53	8,43	0,05	2,13	1,10

Table 4.4: *50/50 (mol) Li_2SO_4/Na_2SO_4*

4.2 XRD - Crystalline Phases and their Thermal Evolution

The results of the characterisation of the powders pre- and post- heat treatment by X-ray diffraction are shown below. This was done to study their microstructure and if any reactivity in the solid state was promoted by the treatment. For each composition (100/0, 79/21, 50/50, 0/100,) the two results are compared.

For the composition 100/0 (mol) Li_2SO_4/Na_2SO_4 (Fig. 4.3) it can be seen that during heat treatment there is only the transformation of $Li_2SO_4*H_2O$ hydrated into Li_2SO_4 anhydrous.

For the composition 79/21 (mol) Li_2SO_4/Na_2SO_4 (Fig. 4.4) it's possible to see the presence of $Li_2SO_4*H_2O$ and after thermal treatment the loss of hydrated salts. Here again there is the presence of $LiNaSO_4$) in both graphs, the formation of which is induced during the ink preparation. The untreated samples also show Na_2SO_4 and $Li_2SO_4*H_2O$. The XRD of the sample after thermal treatment shows only the phases $LiNaSO_4$ and anhydrous Li_2SO_4.

For the composition 50/50 (mol) Li_2SO_4/Na_2SO_4 (Fig. 4.5) there is no change in microstructure. It is interesting to see in the non-heat-treated powder $LiNaSO_4$ and not Li_2SO_4 or Na_2SO_4 or their hydrated forms. This is probably due to the high reactivity of the systems that need only small energy (in this case, mechanical energy and the thermal contribution due to the local increase of the temperature during ink preparation ($Li_2SO_4+Na_2SO_4 \rightarrow LiNaSO_4$) to overcome the energetic barrier of the reaction/transformation [6].

For the composition 0/100 (mol) Li_2SO_4/Na_2SO_4 (Fig. 4.6), no change is noted, there is only the presence of anhydrous Na_2SO_4. Variations in the pattern are noticeable but no change in the final result.
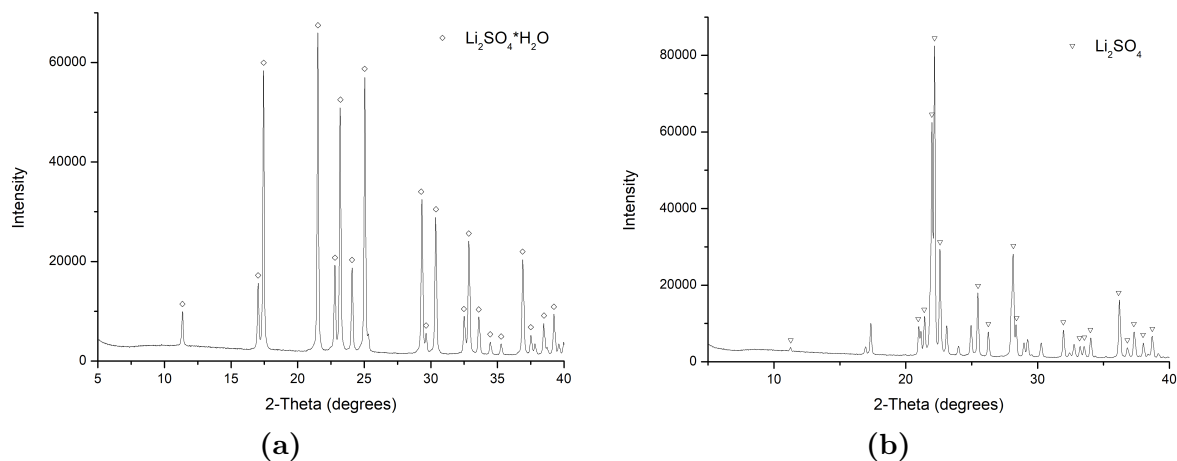

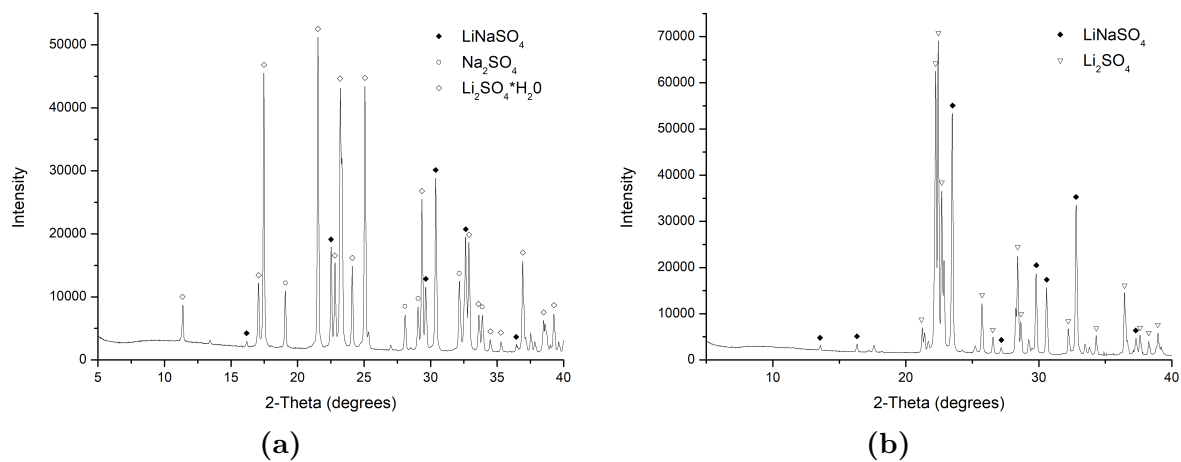**Figure 4.3:** *XRD pattern 100/0: (a) no thermal treatment, (b) thermal treatment 600 °C*

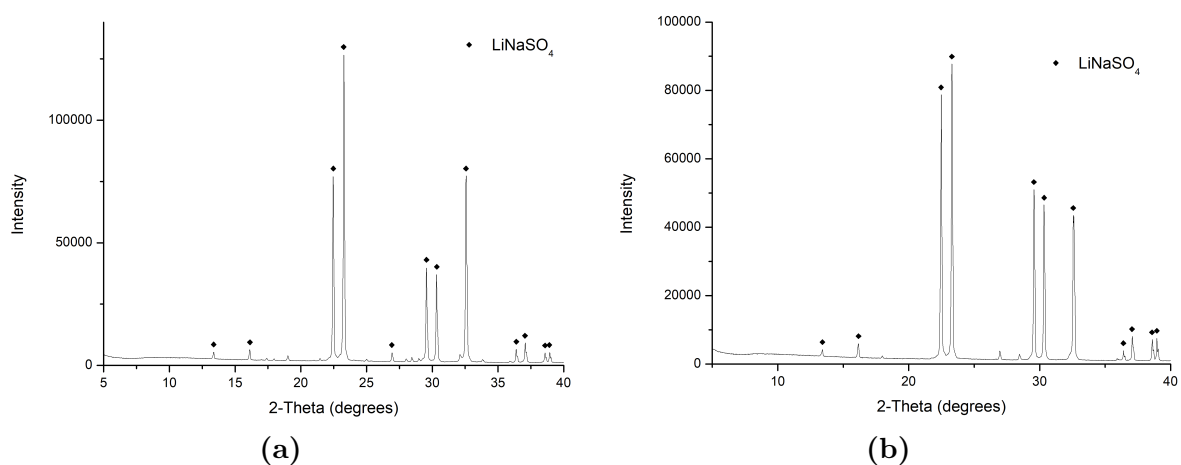**Figure 4.4:** *XRD pattern 79/21: (a) no thermal treatment, (b) thermal treatment 600 °C*

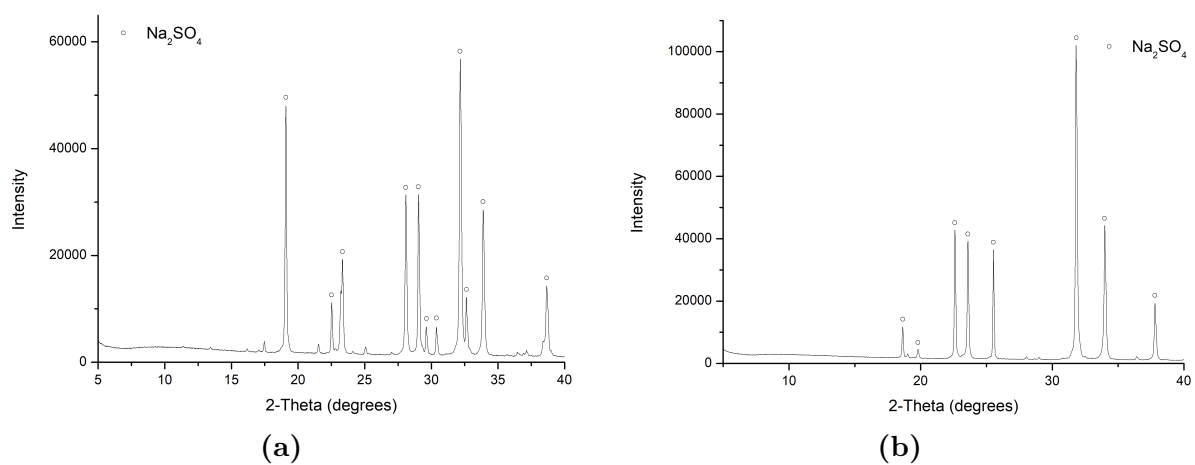**Figure 4.5:** *XRD pattern 50/50: (a) no thermal treatment, (b) thermal treatment 500 °C*

Figure 4.6: *XRD pattern 0/100: (a) no thermal treatment, (b) thermal treatment 600 °C*

4.3 Energy-dispersive X-ray spectroscopy EDS compositions

Energy-dispersive X-ray spectroscopy (EDS) is a technique used to analyze the elemental composition of a sample. It is often used in materials science to determine the presence and distribution of different elements within a sample.

EDS was performed on these different structures:

- 100/0 (mol) Li_2SO_4/Na_2SO_4 before TT

- 79/21 (mol) Li_2SO_4/Na_2SO_4 cross-section before and after the TT

- 79/21 (mol) Li_2SO_4/Na_2SO_4 two different filament surfaces after the TT, one after TT at 500 °c and the other after TT at 600°C

- 50/50 (mol) Li_2SO_4/Na_2SO_4 cross-section before and after the TT

The presence of Lithium will not be detected because the atom is too small. In the analysed images, dark areas are associated with light elements and light areas with heavy elements. Therefore, it can be deduced from the XRD results that the light dots could be Li_2SO_4, $LiNaSO_4$ or Li_2SO_4*xH_2O while the darker dots Na_2SO_4 and Na_2SO_4 hydrate.

In Fig. 4.7 the 100/0 (mol) Li_2SO_4/Na_2SO_4 before thermal treatment is analysed. The pattern shows two high peaks of S and O which can be attributed to Li_2SO_4 and given the high value of the O peak it is appropriate to think at its hydrated form Li_2SO_4*xH_2O. There is also a small presence of carbon due to the presence of burnt PVP.

In Fig. 4.8a the cross-section of 79/21 (mol) Li_2SO_4/Na_2SO_4 before thermal treatment is analysed. There are 3 distinct peaks: oxygen and lithium attributable to Li_2SO_4*xH_2O and there is also Na attributable to Na_2SO_4 and $LiNaSO_4$. This pattern also has carbon due to the presence of PVP. In 4.8b, on the other hand, the same composition was analysed but after heat treatment. The first change that can be seen is that the carbon goes from being present for 10,6 Wt% in the pre-treatment sample to a value of 3,9 Wt%, which means that during heat treatment the binder was almost completely removed. The other peaks, i.e. Na and S remained almost unchanged, increasing slightly in Wt% value while the O Wt% decreased by a little. These elements confirm the presence of $LiNaSO_4$ and Li_2SO_4.

Figure 4.9 shows the surface of the filament of composition 79/21 (mol) Li_2SO_4/Na_2SO_4 after two different heat treatments. The darker specimen, Fig. 4.9a, underwent treatment at 500 °C while the lighter specimen, Fig. 4.9b underwent treatment at 600 °C. The oxygen and sulphur peaks are present in both samples, but only in the dark specimen does the Na peak appear. A consideration can be made from this data: around 600 °C, a liquid phase is probably formed for this 79/21 composition, which is not marked in the theoretical diagram in Fig. 2.3, and therefore the $LiNaSO_4$ formed during the thermal cycle, once it reaches liquidus temperature, changes phase and becomes liquid moving

away from the surface redistributing itself in the section leaving only a homogeneous, light-coloured structure referable to Li_2SO_4.

The last analysis was performed on 50/50 (mol) Li_2SO_4/Na_2SO_4 pre- and post heat treatment. In Fig. 4.10, there are 3 peaks: S, Na and O. This certifies the presence of $LiNaSO_4$. There is also the 11,3Wt% of C always due to the binder. In Fig. 4.10b, after heat treatment, confirming the removal of the binder, there is a 5,8Wt% decrease in the presence of C. The peaks of the other elements remain almost unchanged, confirming the presence of $LiNaSO_4$ here too.
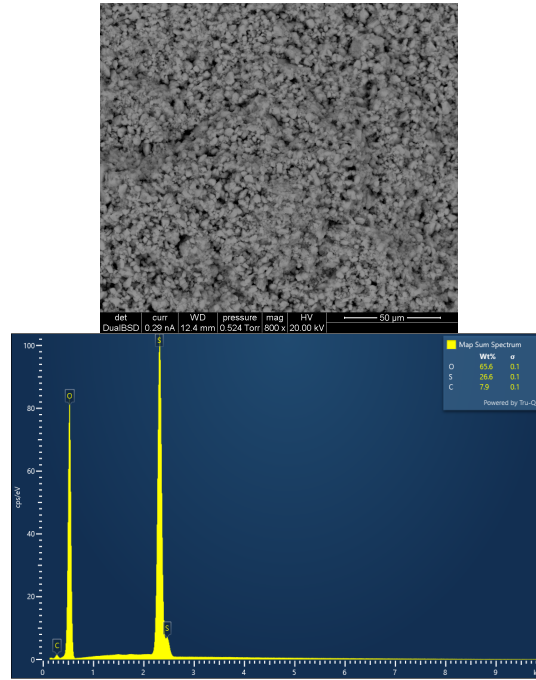
Figure 4.7: *EDS spectrum 100/0 cross-section no TT*

(a)

(b)
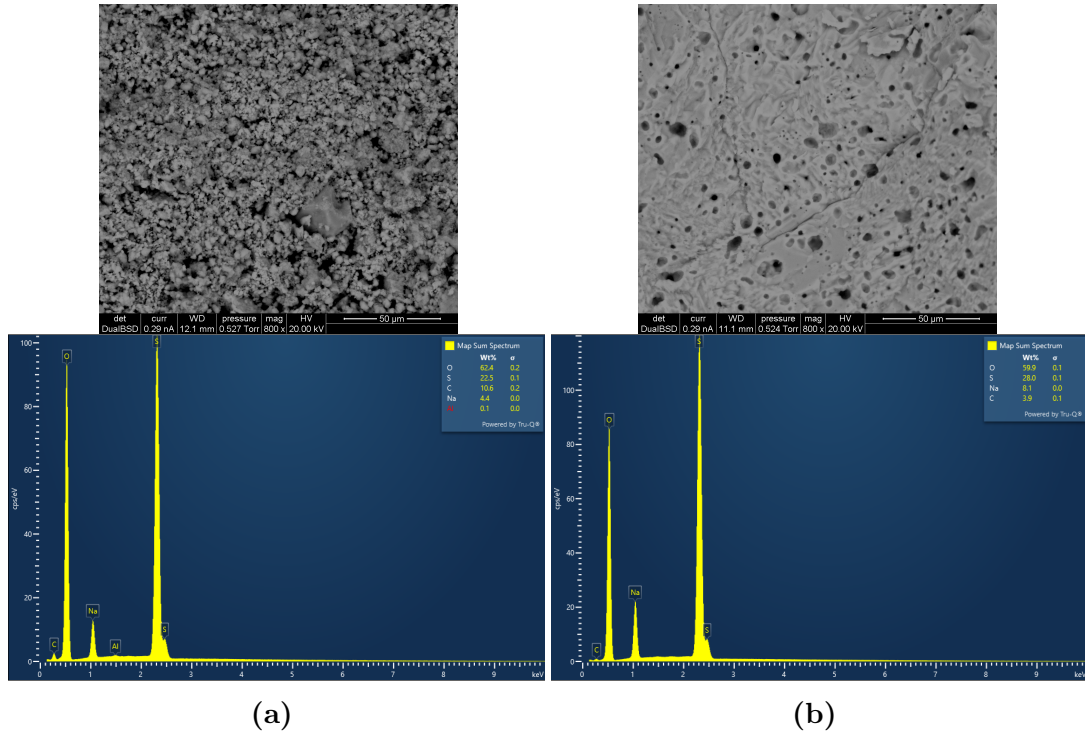
Figure 4.8: *EDS spectrum 79/21 cross-section: (a) no TT, (b) after TT*
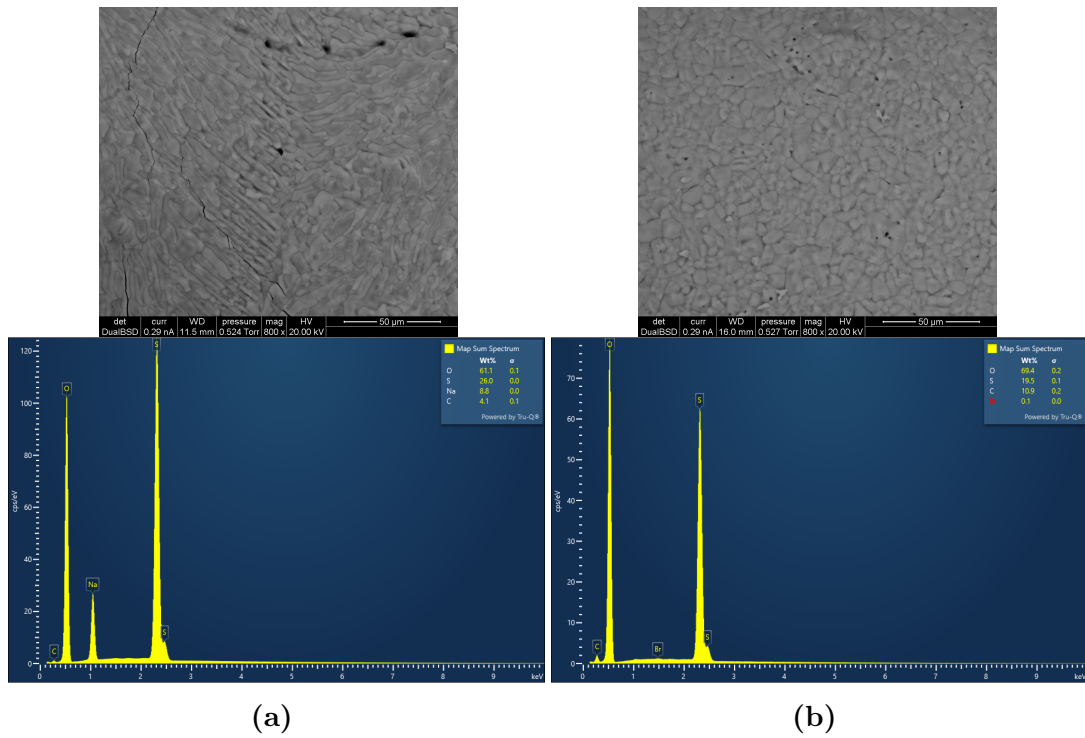

(a)

(b)

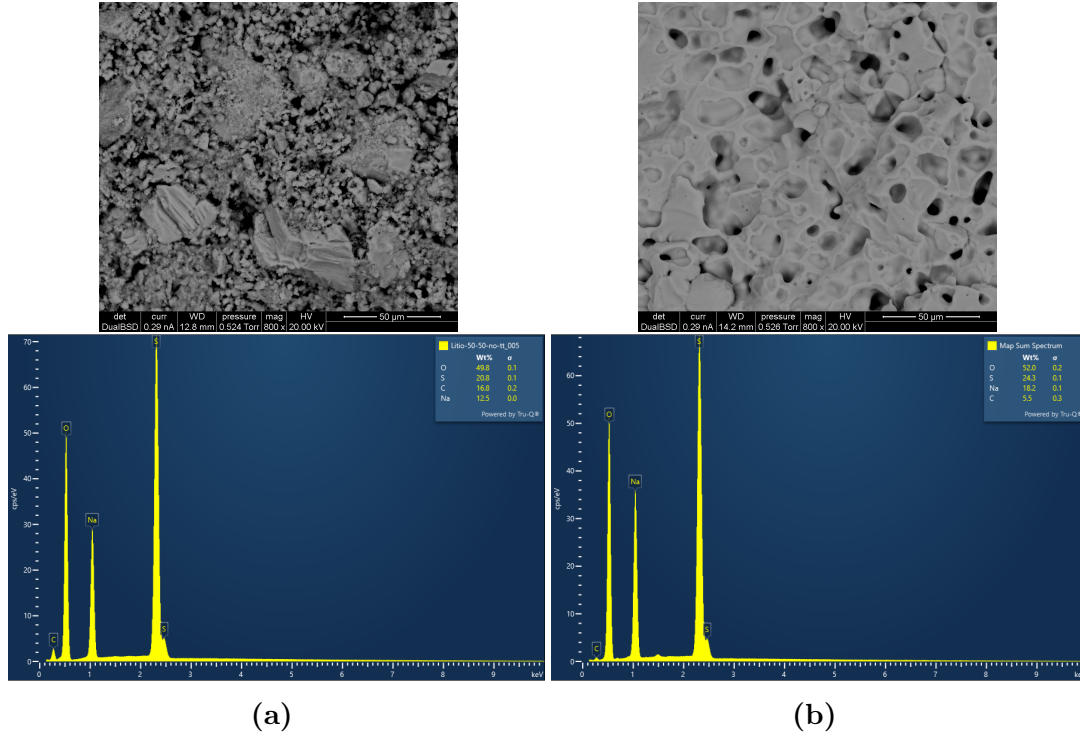**Figure 4.9:** *EDS spectrum 79/21 filament surface TT analysis: (a) 500 °C, (b) 600 °C*

Figure 4.10: *EDS spectrum 50/50 cross-section: (a) no TT, (b) after TT*

4.4 SEM - Microstructures

4.4.1 100/0 (mol) Li$_2$SO$_4$/Na$_2$SO$_4$

The images in Fig. 4.11 refer to a cross-section of 100/0 (mol) Li$_2$SO$_4$/Na$_2$SO$_4$ filament before heat treatment. In the first two images, the first thing that can be noted is a perfectly circular cavity in the centre of the filament with a certain depth. This cavity is the result of an air bubble produced during the printing phase and is elongated, and not spherical, due to the stretching of the ink during this phase. The micro structure is composed of uniformly distributed grains and the EDS structure map (predominantly green image) confirms this showing the uniform distribution of carbon, sulphur and oxygen in the section. The images in Fig 4.12 still refer to the cross-section, but of the heat-treated material. A colour-homogeneous compound is shown, and a more compact structure with an absence of grain boundaries can be seen. However there is a lot of porosity that presents a geometric shape, resembling hexagons. This porosity is probably due to the evaporation of the water present in the hydrated material before treatment. Zooming inside the macro porosity, caused by the probable presence of air bubbles in the ink during printing, one notices grains that having found room for growth, have developed. The last series of images (Fig. 4.13) refer to the outer layer of the filament: heat-treated surface . Here you can see the same structure as inside the macro porosity in the cross-section of the filament (Fig. 4.12). The only difference is the presence of a cluster of crystals caused by not dried ink that has leaked from the filaments above.
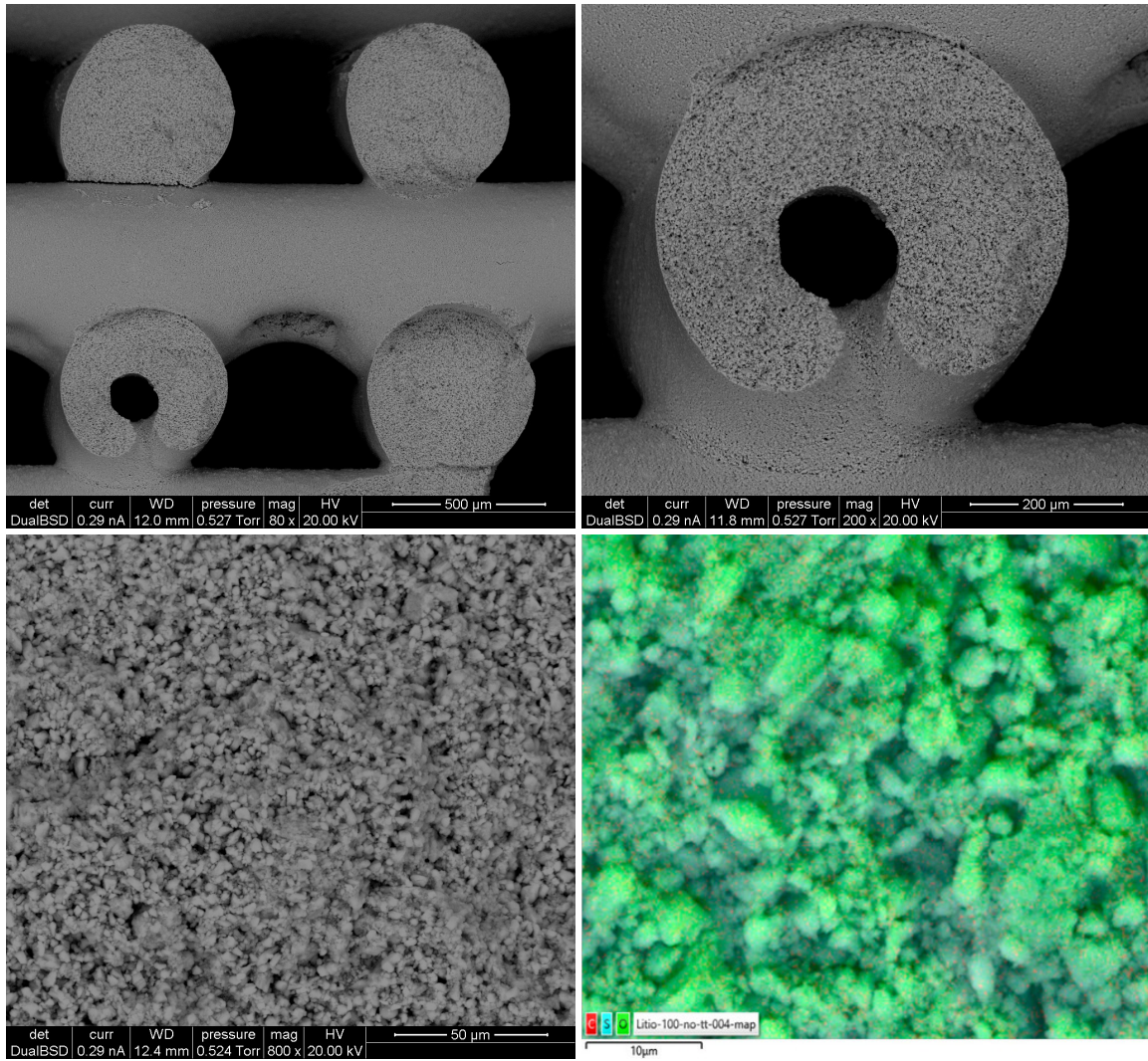
Figure 4.11: *SEM images 100/0 (mol) Li_2SO_4/Na_2SO_4 no thermally treated cross-section, from top left to right: 80x, 200x, 800x, EDS map*

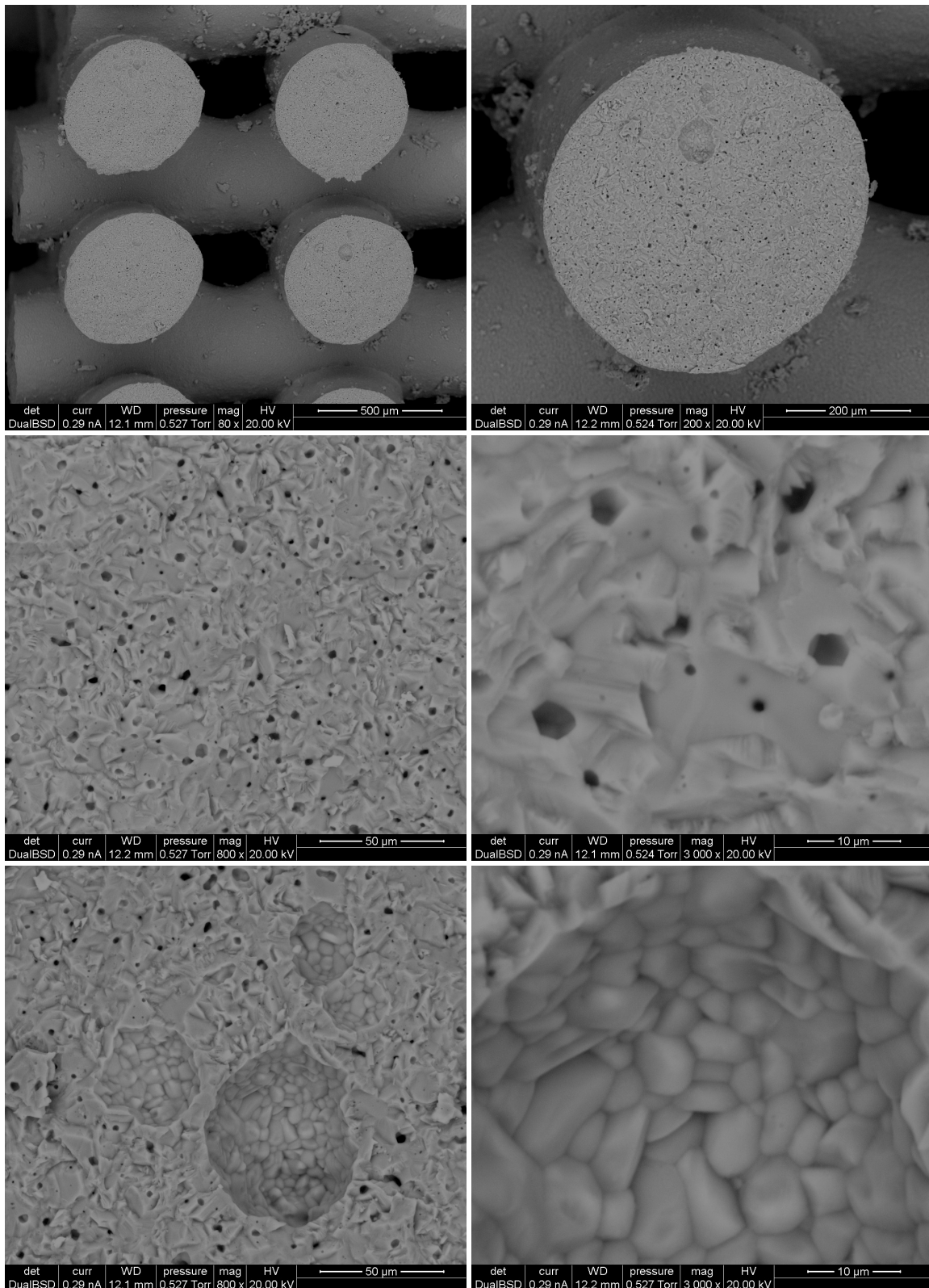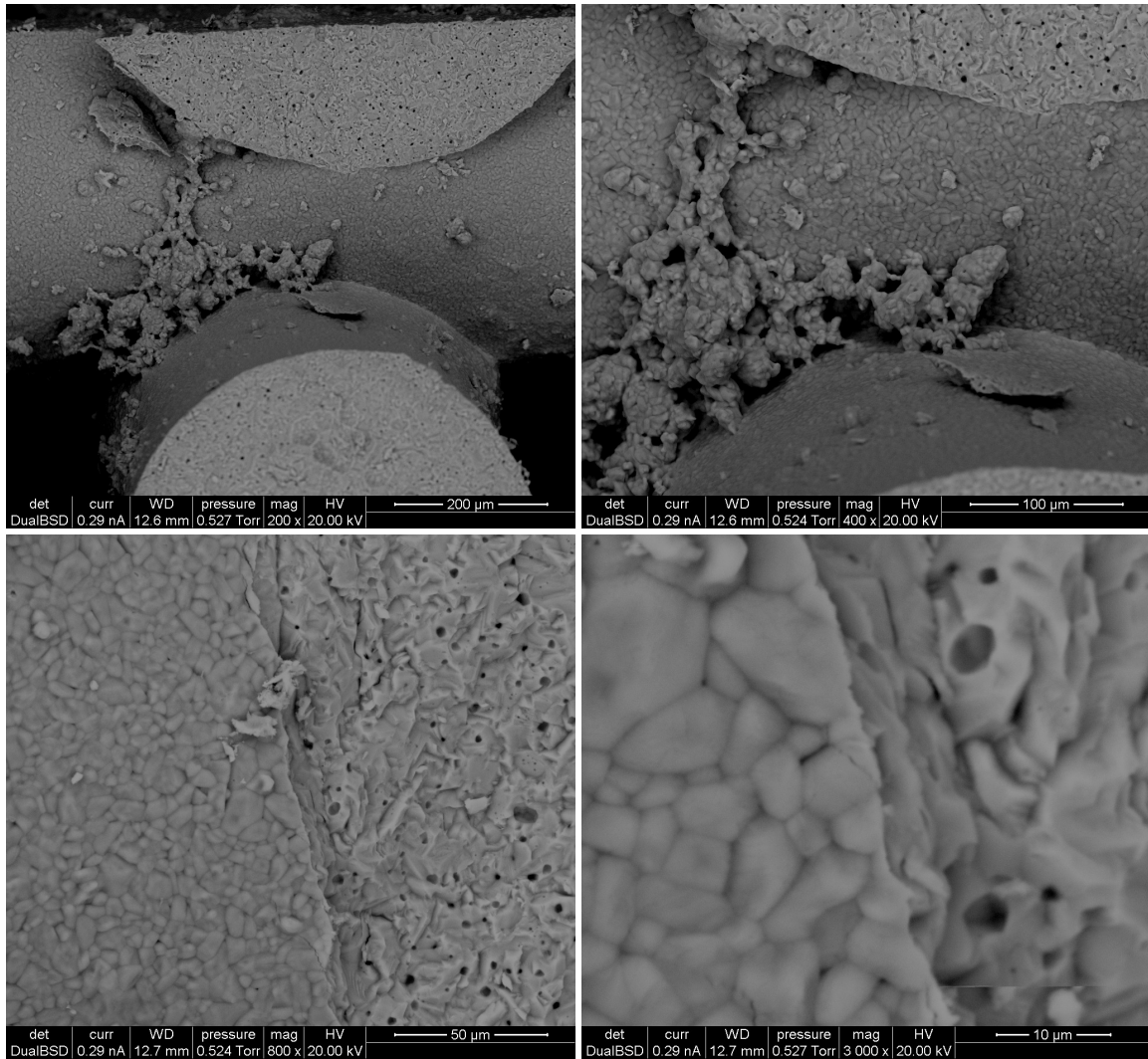**Figure 4.12:** *SEM images 100/0 (mol) Li_2SO_4/Na_2SO_4 thermally treated cross-section, from top left to right: 80x, 200x, 800x, 3000x, 800x, 3000x*

Figure 4.13: *SEM images 100/0 (mol) Li_2SO_4/Na_2SO_4 thermally treated surface, from top left to right: 200x, 400x, 800x, 3000x*

4.4.2 79/21 (mol) Li$_2$SO$_4$/Na$_2$SO$_4$

Fig 4.14 shows the cross-section structure of a sample before heat treatment. The shape of the filament does not appear perfectly circular, possibly due to too slow drying during printing with consequent relaxation of the extruded material. The size of the different grains appears homogeneous as does the distribution of light and dark grains. The EDS map confirms this, as the sulphur is evenly distributed, sodium forms small clusters well distributed. Analysing now the cross section of the treated material, at 600 °C, in Fig 4.15, one notices, in addition to the presence of cavities in the filament caused by bubbles during printing, an amorphous structure with the presence of a few cracks and significant porosity that does not show any particular geometry. The EDS map shows that both sulphur and sodium as well as carbon, present in the binder, are well distributed. Analysing the images of the filament surface, no particular differences in the crystal structure of the untreated material (Fig. 4.16) compared to the cross section (Fig. 4.14) can be seen. In contrast, In Fig. 4.17, a portion of the surface of the filament heat treated at 600 °C is observed, which was lighter to bare eye. A clear globular structure with grains of similar size can be seen and, from the map, is clear that there is no presence of sodium as found by EDS in Fig. 4.9b. An interesting structure, instead, can be seen in the heat-treated material at 500 °C (Fig. 4.18). The grains are narrow, elongated shape oriented in the direction of printing, which is not noticeable in the non-heat-treated samples. The coloured EDS map shows how there is an alternation between grains containing the sodium atom and those without it, creating a zebra-like pattern.
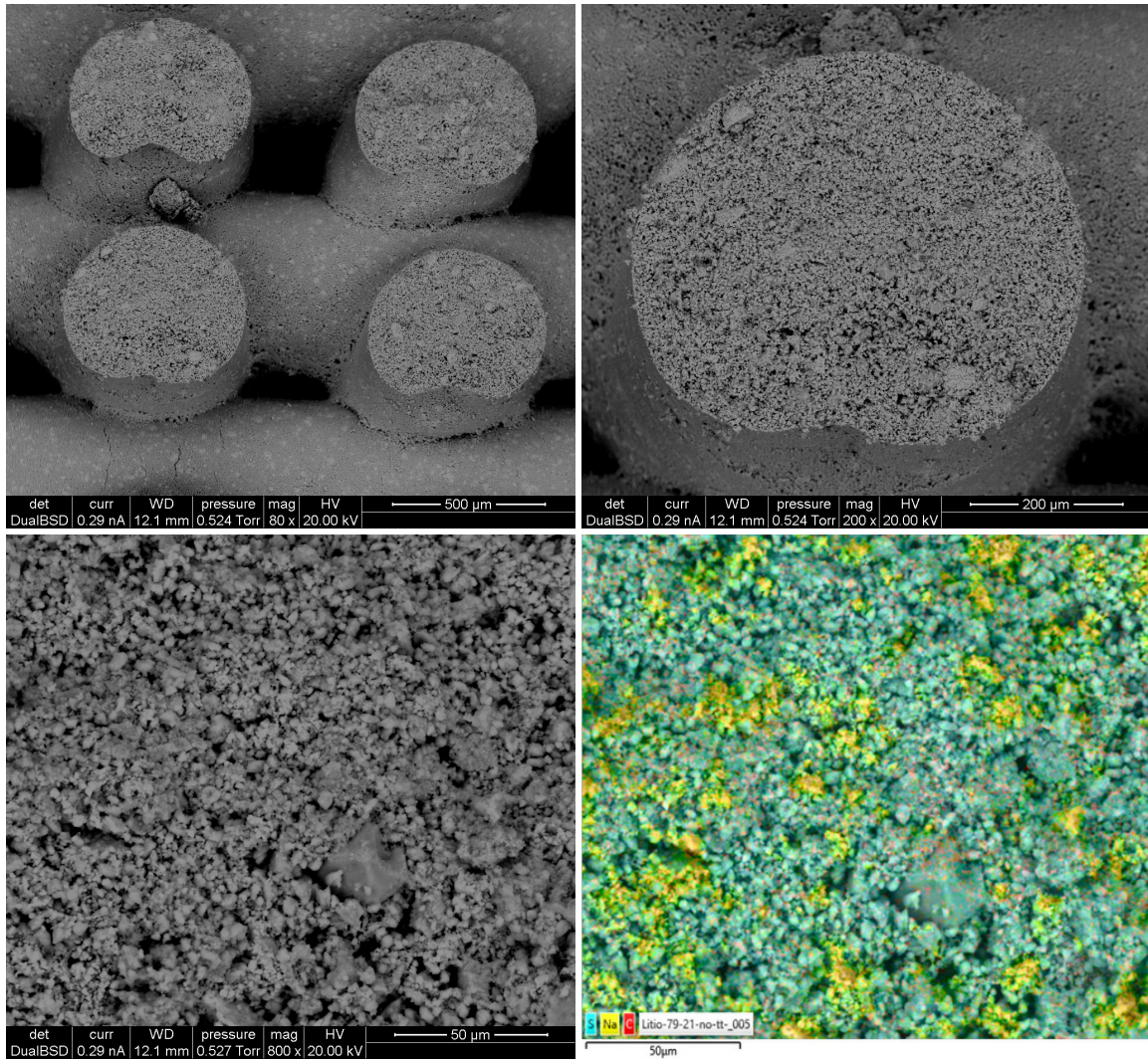
Figure 4.14: *SEM images 79/21 (mol) Li_2SO_4/Na_2SO_4 no thermally treated cross-section, from top left to right: 80x, 200x, 800x, EDS map*
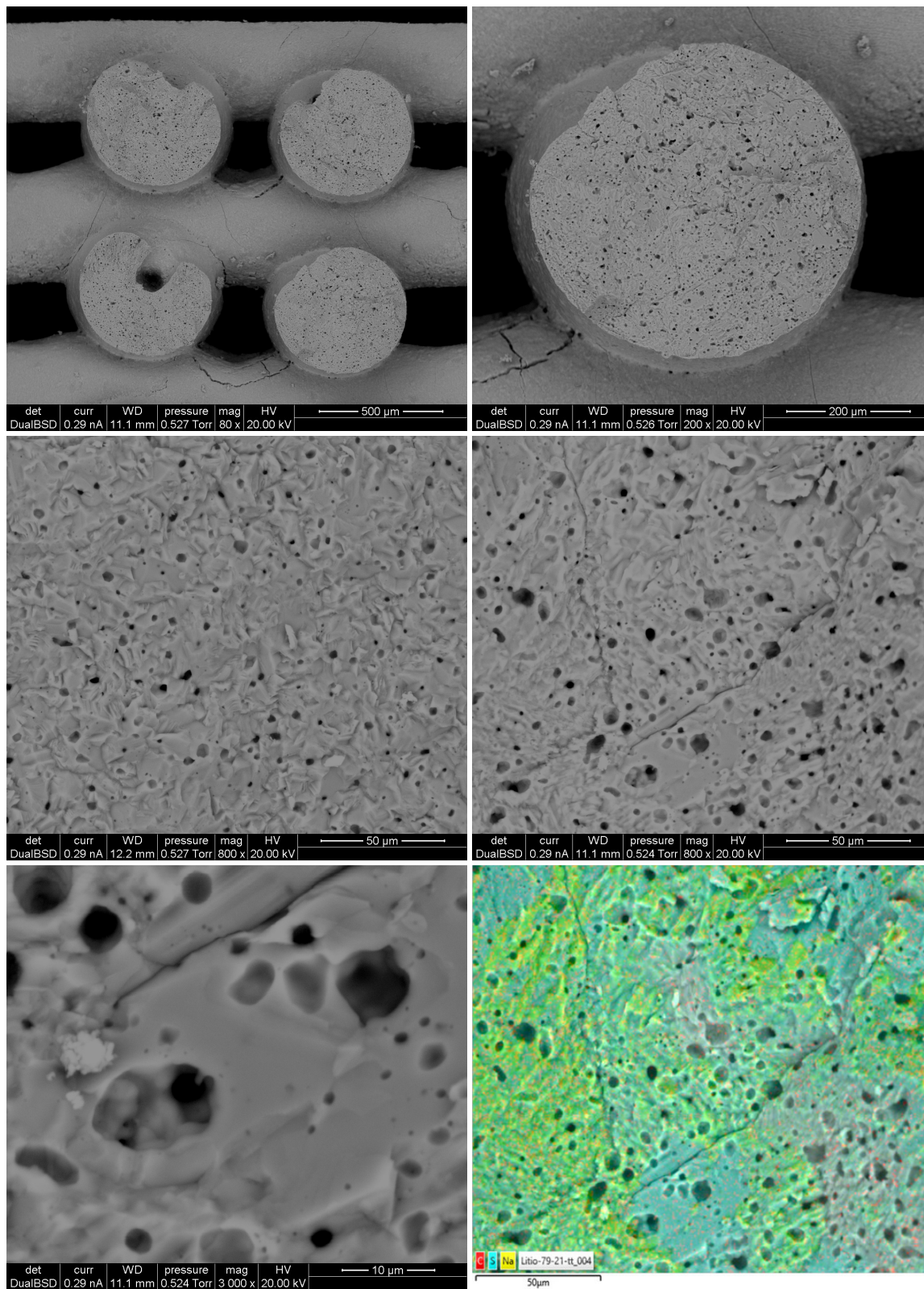
Figure 4.15: *SEM images 79/21 (mol) Li_2SO_4/Na_2SO_4 thermally treated cross-section at 600 °C, from top left to right: 80x, 200x, 800x, 800x, 3000x, EDS map*

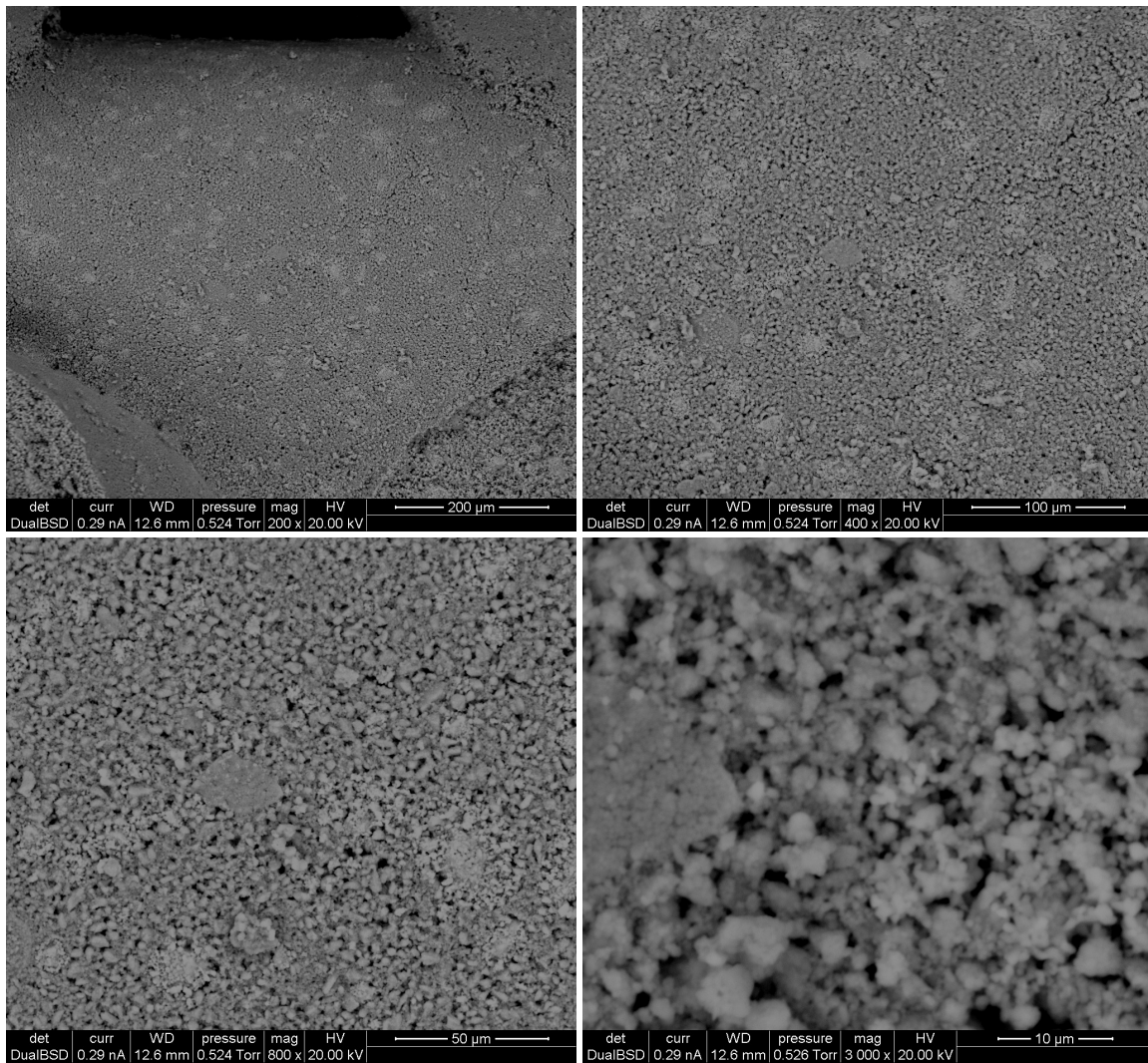**Figure 4.16:** *SEM images 79/21 (mol) Li_2SO_4/Na_2SO_4 no thermally treated surface, from top left to right: 200x, 400x, 800x, 3000x*
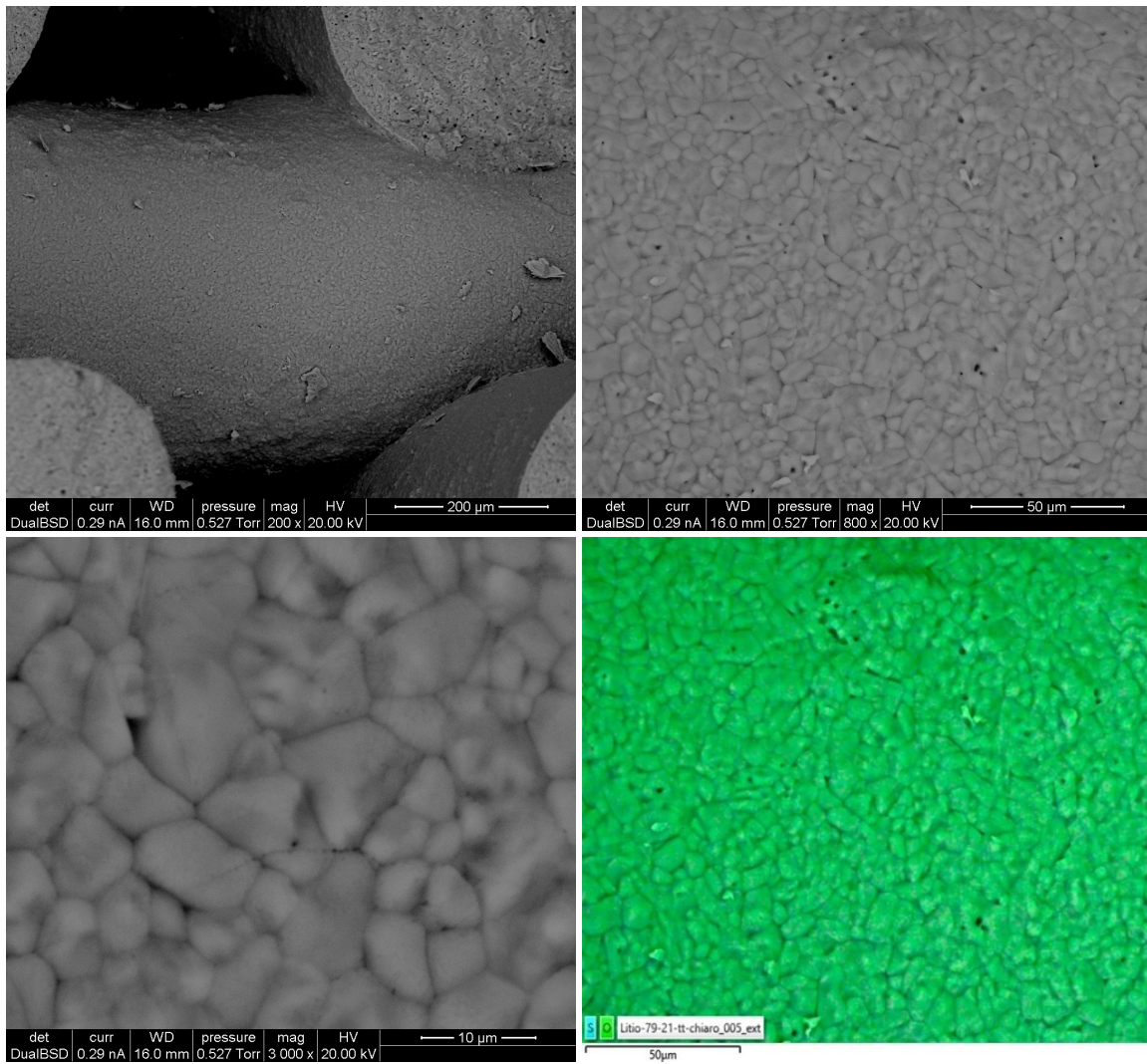
Figure 4.17: *SEM images 79/21 (mol) Li_2SO_4/Na_2SO_4 thermally treated surface at 600 °C, lighter-coloured filament portion, from top left to right: 200x, 800x, 3000, EDS map*
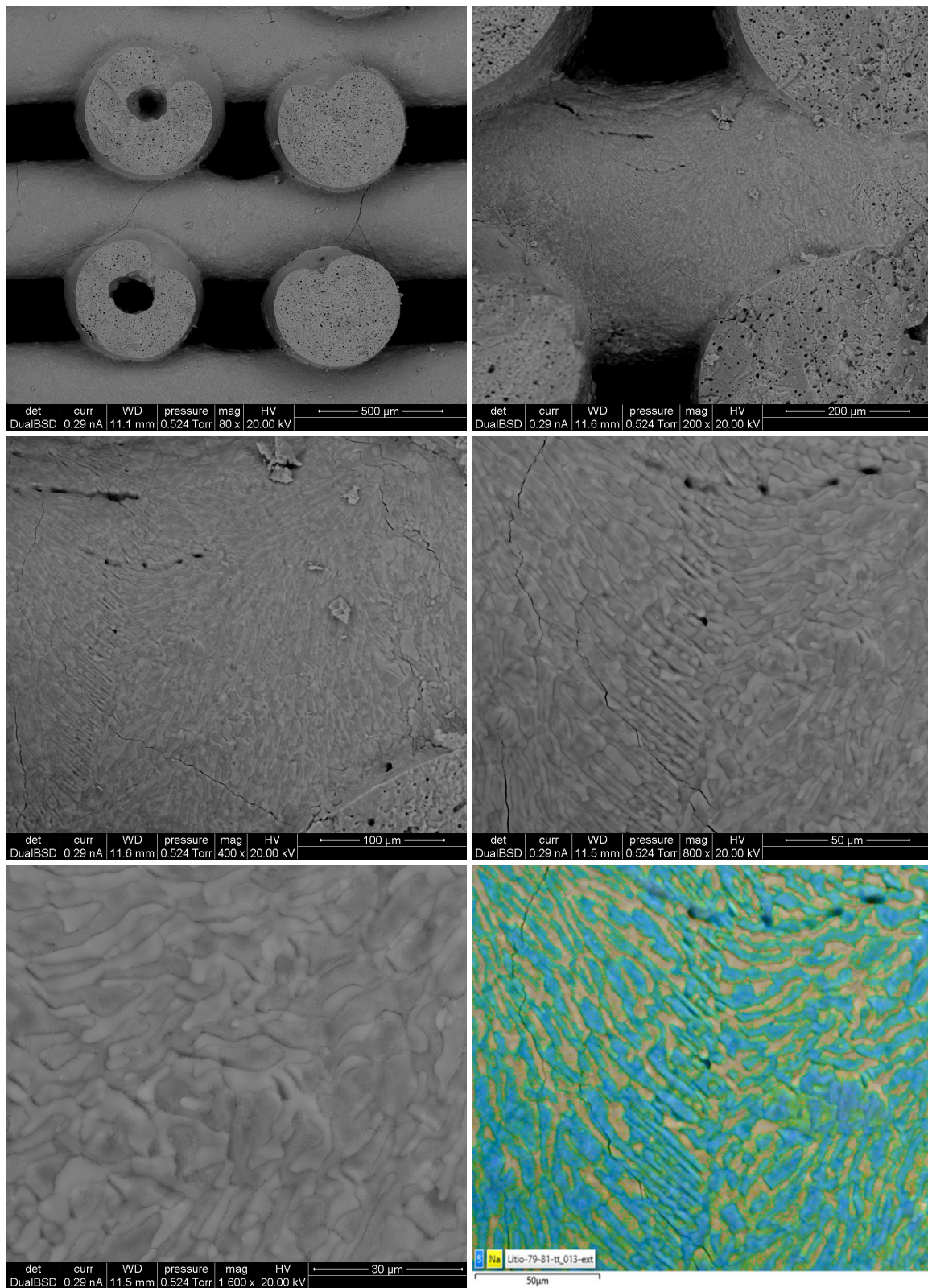
Figure 4.18: *SEM images 79/21 (mol) Li_2SO_4/Na_2SO_4 thermally treated surface at 500 °C, from top left to right: 80x, 200x, 400x, 800x, 1200x, EDS map*

4.4.3 50/50 (mol) Li$_2$SO$_4$/Na$_2$SO$_4$

Image 4.19 shows the cross section of the non-heat-treated sample. In the third image (400x magnification), a large crystal can be seen, almost 100 μm. As the material was sieved at 63 μm there should not be such large crystals, so it is a structure formed after mixing and before printing. The micro structure is not homogeneous: it has small, well distributed crystals with a few randomly distributed abnormal crystals. Sulphur is also present, it was decided to not highlight it on the EDS map in order to show the sodium crystals more clearly. From the map can be seen that the distribution of sodium is uniform, unlike that of carbon which is quite uneven. In the map the grey parts are not due to the absence of sodium but are shaded areas caused by the larger crystals. The structure of the heat-treated cross-section (Fig. 4.20) is an amorphous structure with an evident porosity with a circular shape. There is also a marked presence of cracks. The EDS map shows that, even in this sample, all elements are uniformly distributed in the cross-section. Fig. 4.21 shows images of the non-heat-treated filament surface where the crystals are homogeneously distributed and are also similar in size, unlike those in the section (Fig. 4.19). In the EDS map, where sulphur is purposely not highlighted, a homogeneous distribution of sodium and carbon can be seen. The grey area on the right is due to the cone of shadow produced by the filament above. The last series of images in Fig. 4.22 show the surface of the treated filament. One can see a compact, smooth, amorphous structure with the presence of a few cracks and some asperities. This is due to the fact that this composition, being the eutectic one, has a lower liquidus temperature than the two salts taken individually, and that, consequently, with treatment at 500 ℃ there is a transition from crystalline to amorphous phase due to the change in crystal structure.

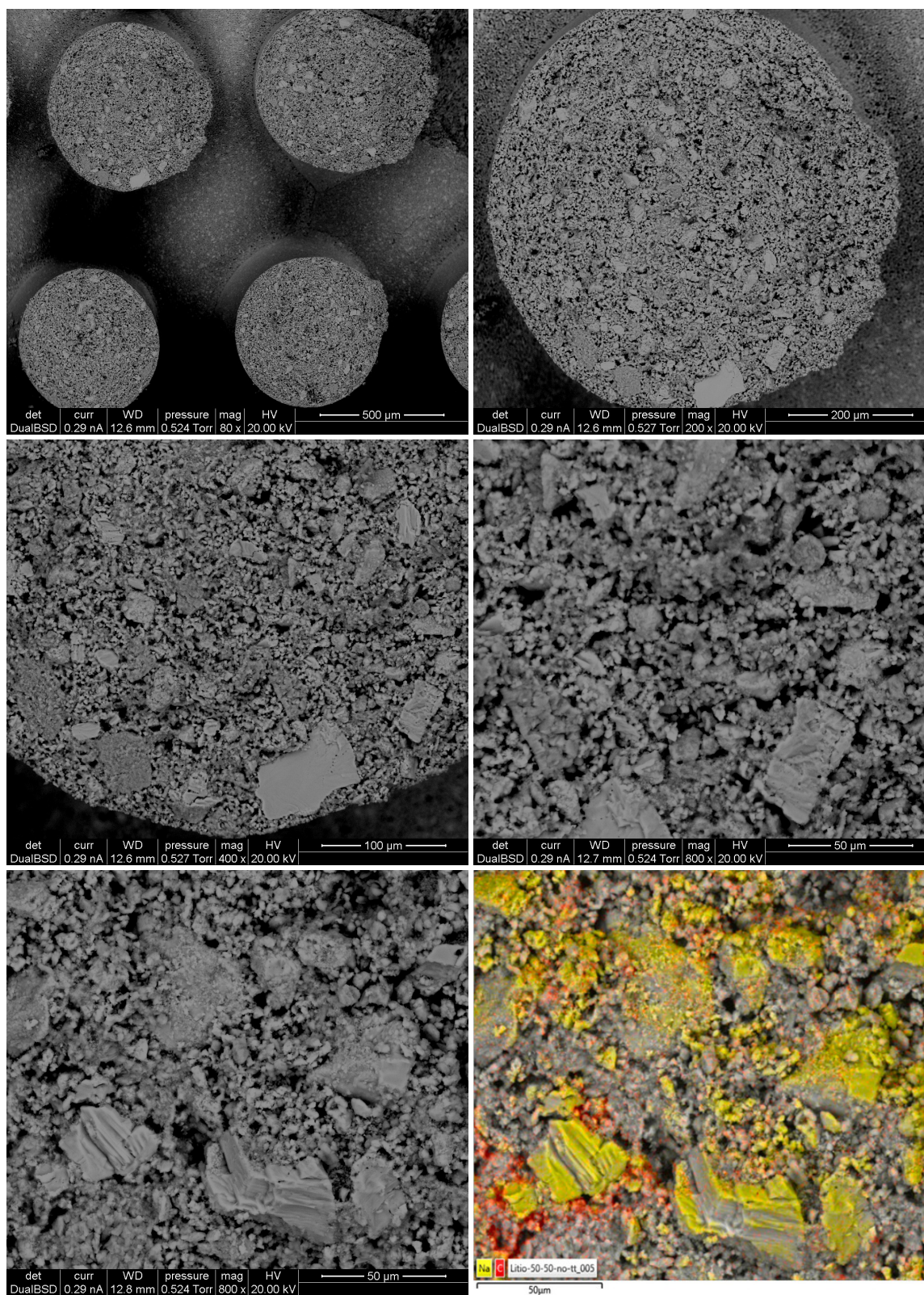**Figure 4.19:** *SEM images 50/50 (mol) Li_2SO_4/Na_2SO_4 no thermally treated cross-section, from top left to right: 80x, 200x, 400x, 800x, 800x, EDS map*

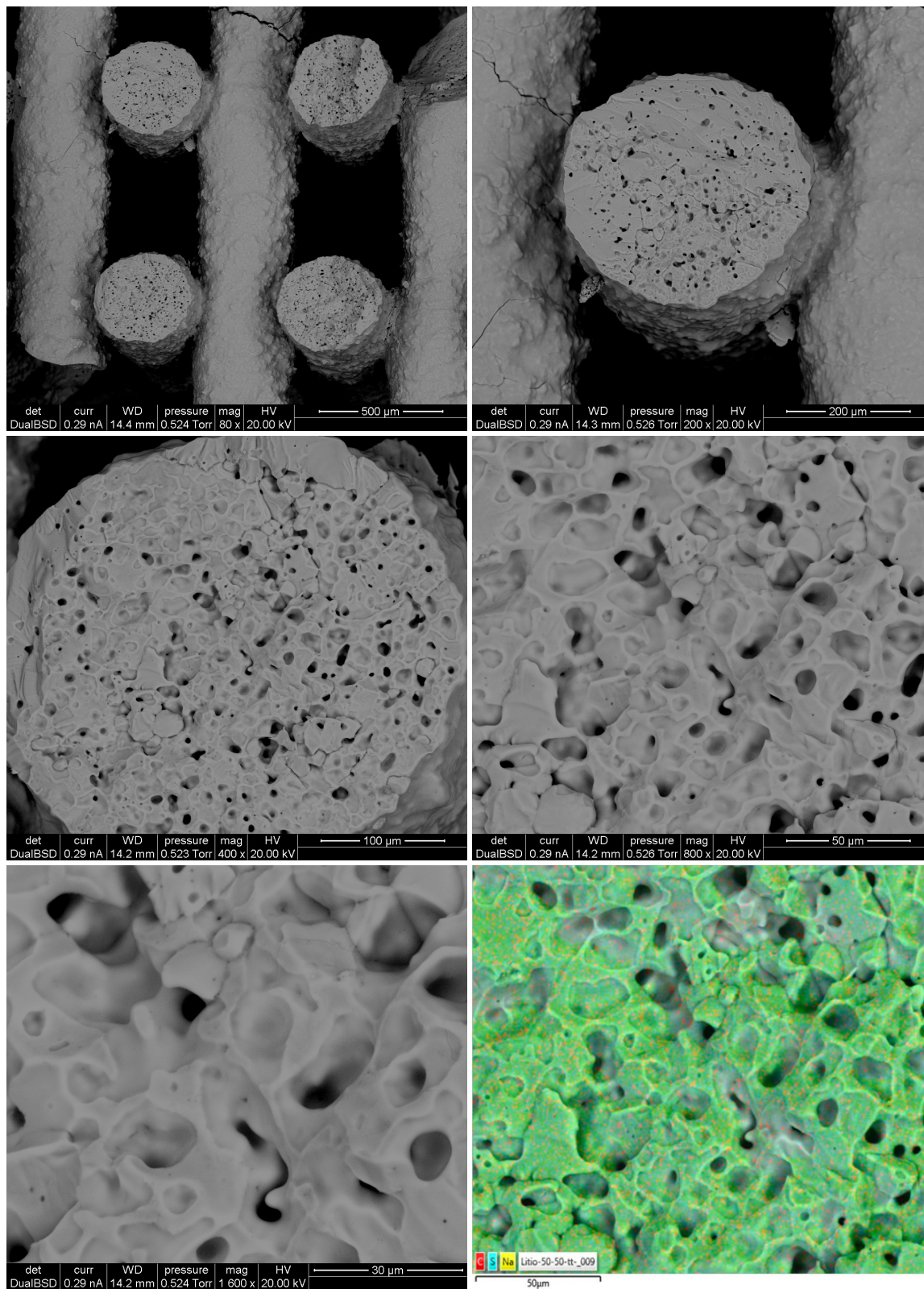**Figure 4.20:** *SEM images 50/50 (mol) Li_2SO_4/Na_2SO_4 thermally treated cross-section, from top left to right: 80x, 200x, 400x, 800x, 1600x, EDS map*

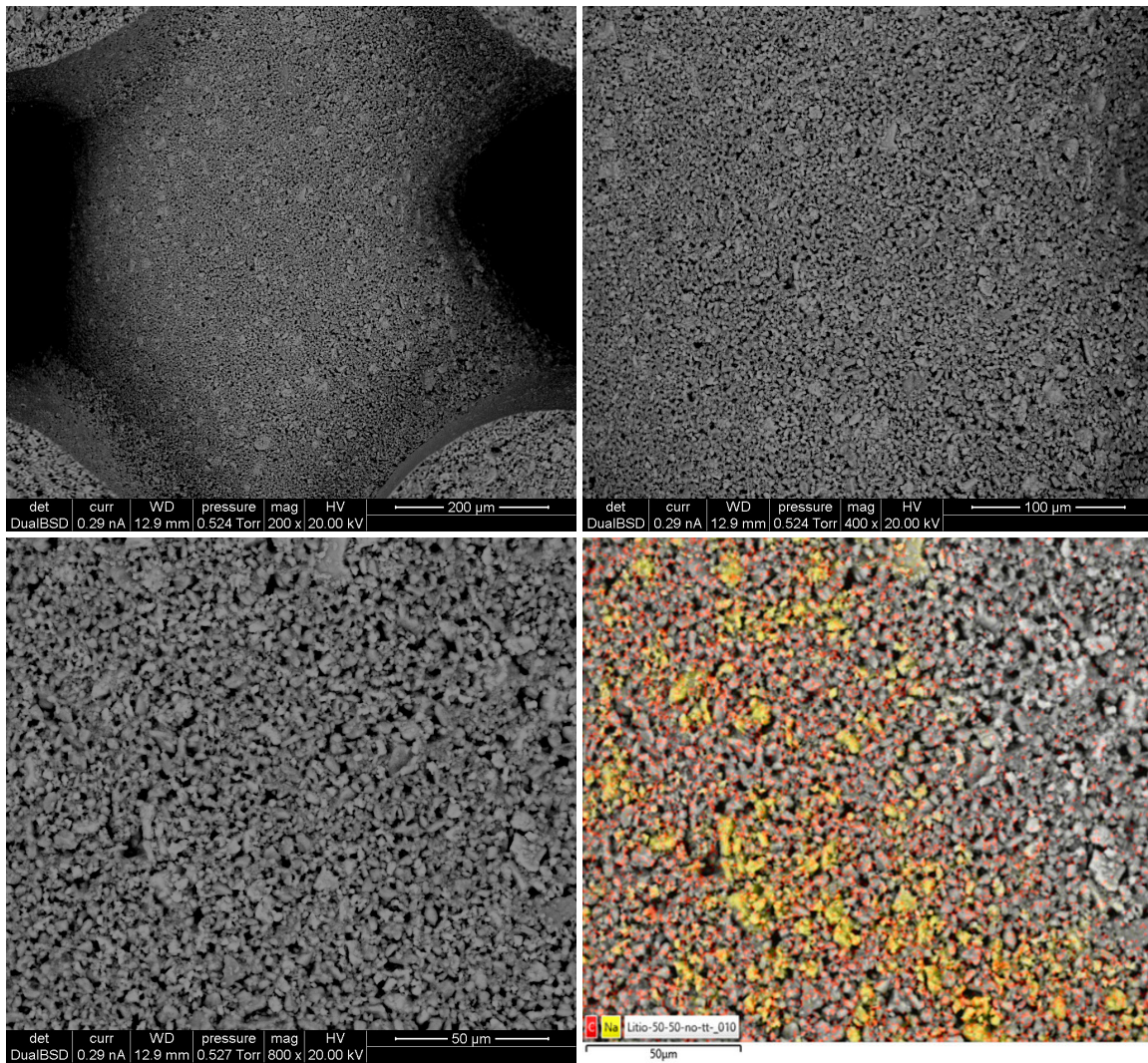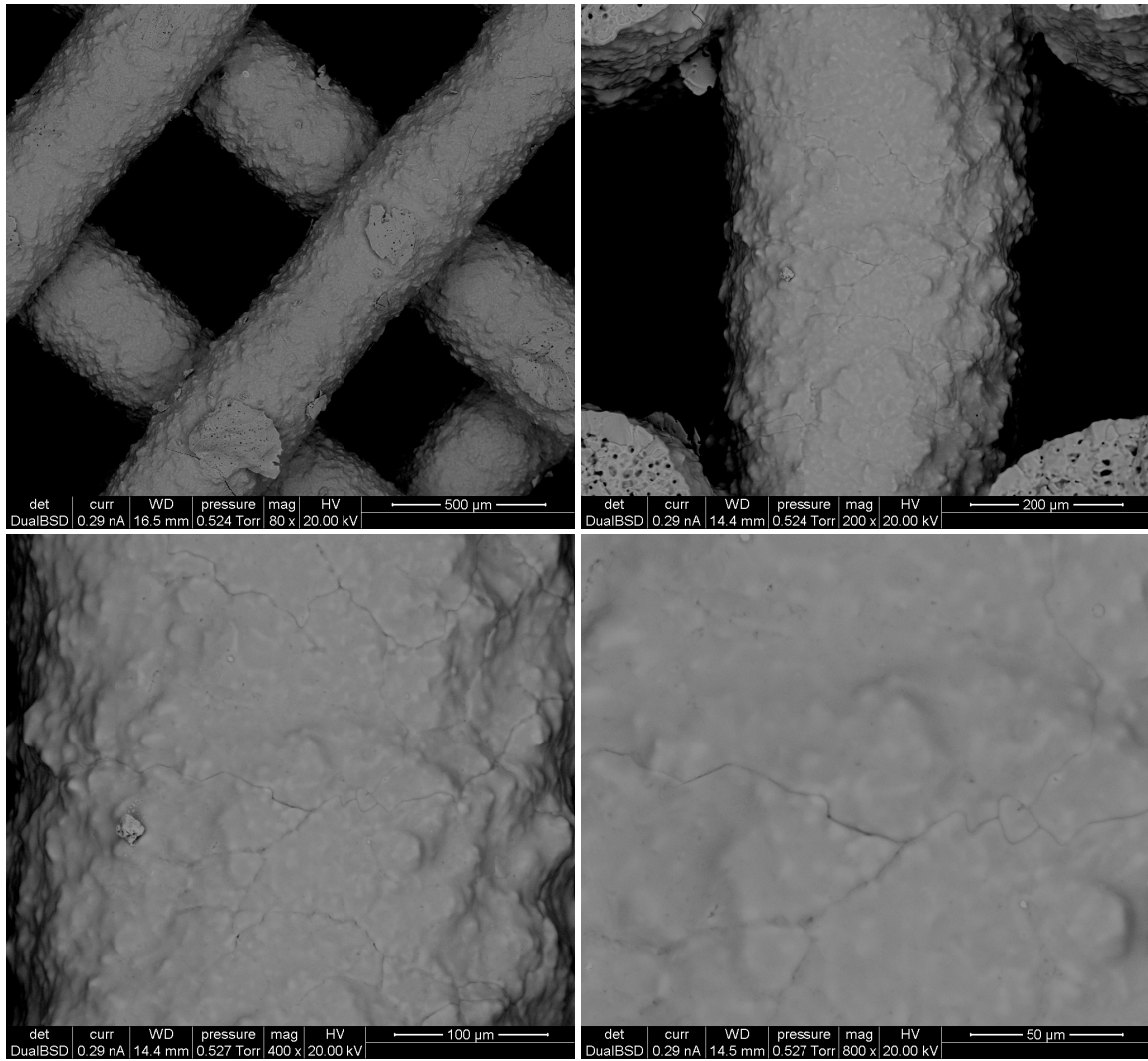**Figure 4.21:** *SEM images 50/50 (mol) Li_2SO_4/Na_2SO_4 no thermally treated surface, from top left to right: 200x, 400x, 800x, EDS map*

Figure 4.22: *SEM images 50/50 (mol) Li_2SO_4/Na_2SO_4 thermally treated surface, from top left to right: 80x, 200x, 400x, 800x*

4.5 DSC and TGA - Pattern analysis

To conduct DSC and TGA, it was chosen to operate in air, and not argon or nitrogen, in order to evaluate materials evolution in an environment similar to that of possible use. The heating curve chosen is from room temperature, T_{amb}=28 °C, up to 400 °C with a heating rate of 10 °C/min to enhance the visibility of thermal events.

Graph 4.23 is the DSC from which any loss of weight of the sample due to combustion, evaporation, melting, etc. can be seen. Graph 4.24, on the other hand, is the TGA graph where the normalised heat flow is expressed on the y-axis. The trend in this graph, it is possible to determine what is happening inside the sample: whether it is an exothermic reaction (positive flow) or an endothermic one (negative flow).
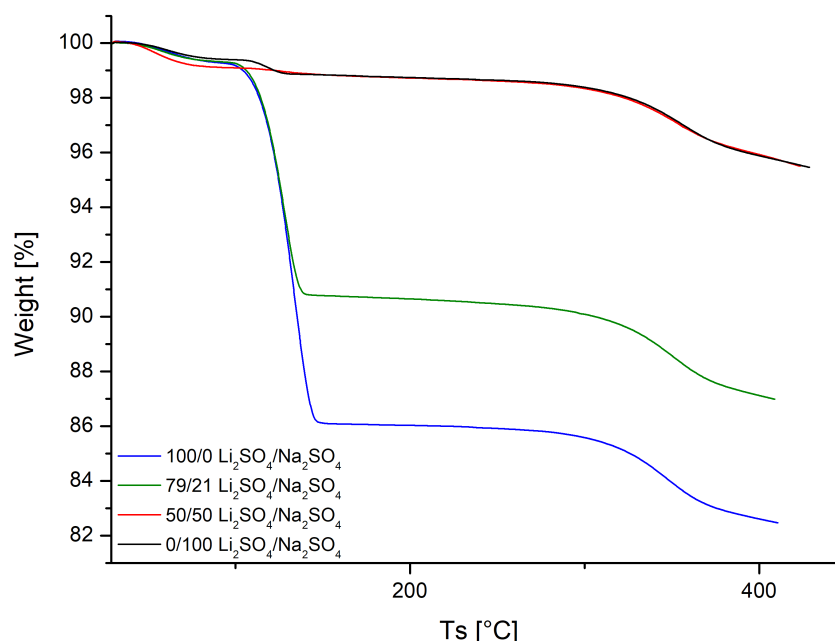

Figure 4.23: *DSC pattern*

Looking at the graph 4.23, there is a weight loss of about 13% at 130 °C in the 100/0 (mol) Li_2SO_4/Na_2SO_4 and 79/21 (mol) Li_2SO_4/Na_2SO_4 samples. The $Li_2SO_4*xH_2O$, which is present in both untreated samples, has a melting temperature of 130 °C and comparing the TGA graph 4.24 is confirmed to be an endothermic event coinciding with the water evaporation. The observed weight loss can be attributed to the dehydration of the material. At a temperature of 270 °C, a second endothermic peak is observed, only in 0/100 (mol) Li_2SO_4/Na_2SO_4, corresponding to a crystalline solid-solid phase transition from $T-Na_2SO_4$ to $\gamma-Na_2SO_4$. Another weight loss, of about 4%, occurs at 315 °C on all 4 samples analysed, and looking at the TGA graph matches with an exothermic peak. Having this reaction on all 4 samples can be assumed to be the combustion of PVP. Since it is present in the mixtures at around 4-5%, as can be seen in the ink formulations in section 3.2, the weight loss, in almost the same percentage, confirms this hypothesis.
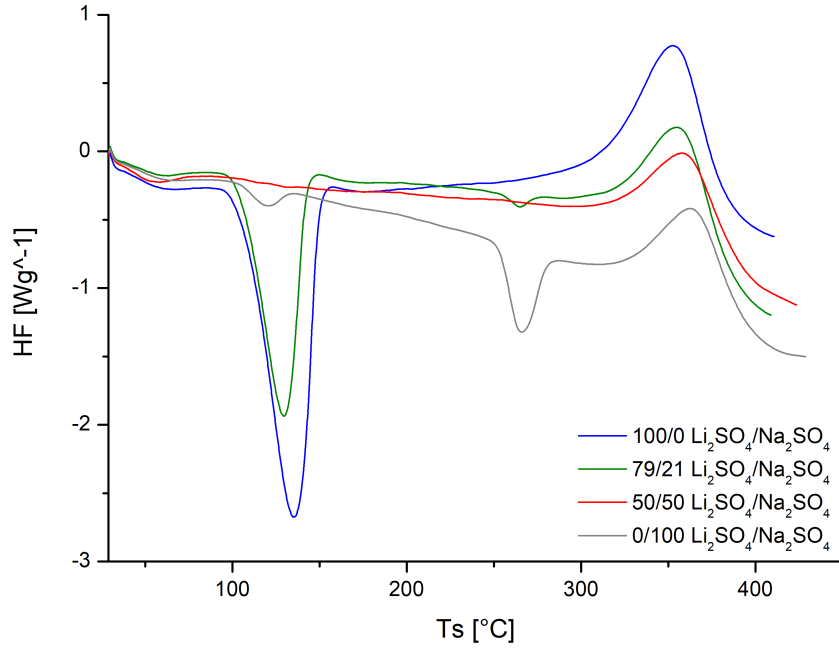
Figure 4.24: *TGA pattern*

4.6 Rheometry analysis

The rheometer used is stress-controlled, i.e. the instrument is able to apply a certain shear stress and measure the corresponding shear rate or deformation. The shear rate for a fluid is defined by:

$$\gamma = \frac{v}{h} \tag{4.1}$$

where γ is the shear rate measured in reciprocal second, v is the velocity of the moving plate, measured in meters per second and h is the distance between the two parallel plates, measured in meters. The shear viscosity of a system measures is resistance to flow. The shear stress, instead, is the component of stress coplanar with a material cross section. The graphs below show the behaviour of the ink in terms of shear viscosity or shear stress as a function of deformation rate. Three inks were analysed, relatively 100/0, 79/21 and 50/50 (mol) Li_2SO_4/Na_2SO_4. By analysing the graphs, considerations can be made about the rheology of the different inks (Fig.4.25):

- 100/0 (mol) Li_2SO_4/Na_2SO_4
    - shear rates 0.1-2 s^{-1}: it exhibits shear-thinning behaviour
    - shear rates 3-40 s^{-1}: it exhibits shear-thickening behaviour
    - shear rates 30-300 s^{-1}: it exhibits shear-thinning behaviour

- 79/21 (mol) Li_2SO_4/Na_2SO_4
    - shear rates 0.1-20 s^{-1}: slightly shear-thickening behaviour (approximate Newtonian behaviour)

– shear rates 20-60 s^{-1}: it exhibits shear-thinning behaviour

- 50/50 (mol) Li$_2$SO$_4$/Na$_2$SO$_4$
    - shear rates 0.1-3 s^{-1}: it exhibits slightly shear-thinning behaviour (approximate Newtonian behaviour)
    - shear rates 3-20 s^{-1}: it exhibits slightly shear-thickening behaviour (approximate Newtonian behaviour)
    - shear rates 20-50 s^{-1}: it exhibits shear-thinning behaviour

To facilitate printing, it is best to stay in the shear rate ranges in which the ink exhibits slightly shear-thinning or Newtonian behaviour and avoid the shear-thickening ranges. Analysing the graphs, it can be seen that with these three compositions, the best solution is to print at low shear rates in a range from 0.3 to a maximum of 2 s^{-1} so as to be able to exploit the pseudoplastic or Newtonian behaviour, avoiding the dilatant behaviour that would make printing more difficult.
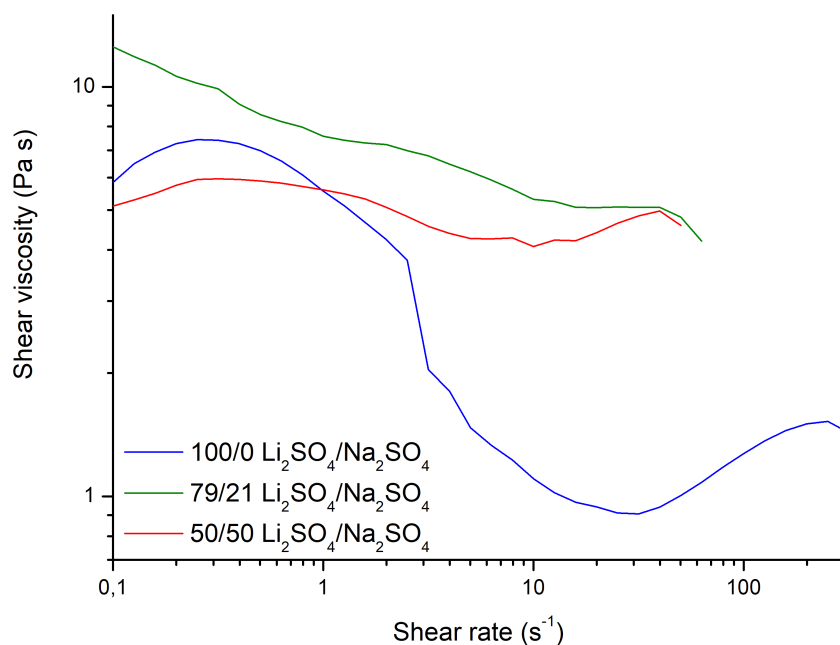

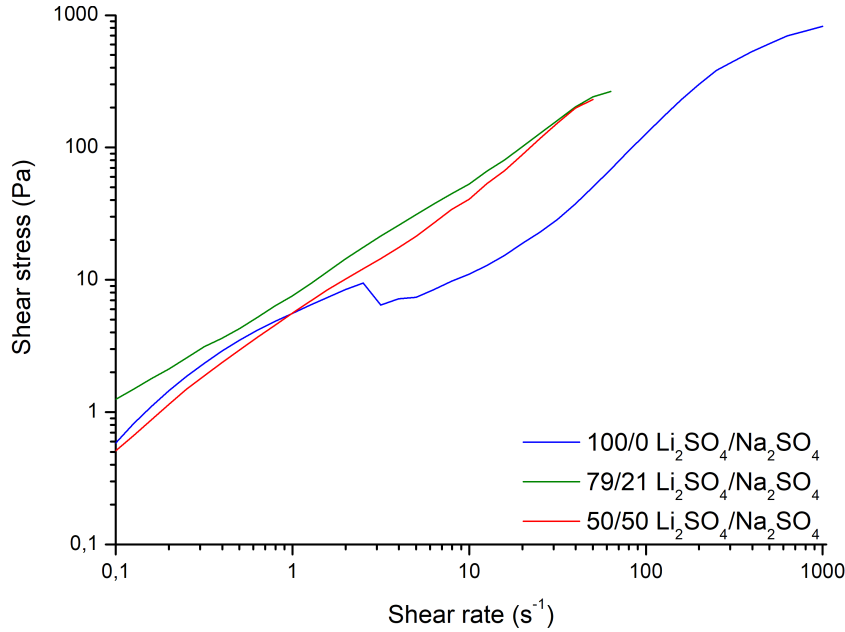**Figure 4.25:** *Shear viscosity vs Shear rate*

Figure 4.26: *Shear stress vs Shear rate*

4.7 Pycnometry analysis

Density analyses were carried out on both heat-treated and non-heat-treated powders and scaffold samples. The gas used is Helium. All the data are presented in the next tables. By increasing the amount of Na_2SO_4 the density of the sample increases, having a density of 2.66 g/cm^3 compared to Lithium which has a density of 2.22 g/cm^3. The dust density of the 100/0 (mol) Li_2SO_4/Na_2SO_4 samples (Tab. 4.5) is not that of the pure material because PVP is present in the powders, which, having a density of 1.22 g/cm^3, inevitably lowers the density. In all three blends analysed, we can see a similar trend, i.e. the powder always has a higher density than the scaffold, both pre- and post-treatment, because the structure of the moulded filament is disordered and has spaces between the grains, and consequently the density is reduced. Heat-treated powders and scaffolds are always less dense than their untreated counterparts. This can be explained by 3 factors:

- Formation of $LiNaSO_4$ in the 50/50 and 79/21 specimens, which is less dense than Na_2SO_4 and thus reduced density

- Development of porosity in treated scaffolds

- The untreated samples show a morphology with smaller particles than the treated ones in which, even with the SEM, a more amorphous structure can be seen. The grain boundaries are not clearly visible (Fig. 4.19 vs Fig. 4.20). Since the powders are obtained by manually grinding monoliths with a mortar, it may be that the untreated powder forms a more compact and dense compound than the heat-treated powders inside the instrument's sample holder

Material type	Density (g)/cm^3
Powder no thermal treatment	2,122 ± 0.229%
Powder thermal treatment 600 °C	2,072 ± 0,029%
Monolith no thermal treatment	2,070 ± 0,102%
Monolith thermal treatment 600 °C	2,094 ± 0,007%

Table 4.5: *Density of 100/0 (mol) Li_2SO_4/Na_2SO_4*

Material type	Density (g)/cm^3
Powder no thermal treatment	2,281 ± 0.027%
Powder thermal treatment 600 °C	2,176 ± 0,027%
Monolith no thermal treatment	2,244 ± 0.145%
Monolith thermal treatment 600 °C	2,058 ± 0,041%

Table 4.6: *Density of 79/21 (mol) Li_2SO_4/Na_2SO_4*

Material type	Density (g)/cm^3
Powder no thermal treatment	2,581 ± 0.054%
Powder thermal treatment 500 °C	2,357 ± 0,057%
Monolith no thermal treatment	2,349 ± 0,029%
Monolith thermal treatment 500 °C	2,120 ± 0,131%

Table 4.7: *Density of 50/50 (mol) Li_2SO_4/Na_2SO_4*

5 Conclusions

The aim of this thesis work was to design, produce and characterise structured Li_2SO_4-Na_2SO_4 scaffolds with additive manufacturing technology, mainly direct ink writing. When the right composition of the 4 inks was found: 100/0 (mol) Li_2SO_4/Na_2SO_4, 79/21 (mol) Li_2SO_4/Na_2SO_4, 50/50 (mol) Li_2SO_4/Na_2SO_4, 0/100 (mol) Li_2SO_4/Na_2SO_4, the production of the test specimens was carried out. Several aspects can be said about the characterisation data:

- Before printing, the ink must run a degassing cycle inside the syringe in order to avoid cavities inside the filaments due to the presence of air bubbles inside the ink once extruded from the nozzle. This could, theoretically, lead to an increase in mechanical properties due to the increased cross-sectional strength.

- SEM images show compact, homogenous structures after heat treatment. EDS analysis also adds the information that the elements are homogeneously distributed throughout the cross-section of the filament, presenting no clusters or ogglomerates.

- Samples with a 50/50 (mol) Li_2SO_4/Na_2SO_4 composition were treated at T= 500 °C to avoid the liquidus T at 613 °C.

- Specimens with composition 79/21 (mol) Li_2SO_4/Na_2SO_4 should be heat-treated between 500 and 550 °C because at 600 °C there is the formation of liquid phase of $LiNaSO_4$ which moving away from the surface redistributing itself in the section. This theoretically should lower the heat transfer efficiency as the superionic conductor is only in a limited part of the specimen.

- The weibull modules of the specimens are relatively low. The values of the moduli are given here: 100/0 (mol) Li_2SO_4/Na_2SO_4 have a m=2.52, 79/21 (mol) Li_2SO_4/Na_2SO_4 have a m=2.23, 50/500 (mol) Li_2SO_4/Na_2SO_4 have a m=1,27.

- From the rheology data, it can be seen that printing at low pressures, and thus low shear rates, results in approximate Newtonian behaviour of the inks, making them easier to print.

- It can be seen, from the XRD patterns, that the heat treatment is effective. First of all, all the hydrated parts are removed so as to leave the scaffold free of impurities. It can then be seen that in the 50/50 (mol) Li_2SO_4/Na_2SO_4 composition remains the presence of only the superionic conductor $LiNaSO_4$ and in the 79/21 (mol) Li_2SO_4/Na_2SO_4 composition there is the formation of $LinaSO_4$ resulting in the total transformation of the Na_2SO_4.

- It can be seen from the DSC graphs that for the complete dehydration of the salts, heat treatment at about 160 ℃ would be sufficient, but for the complete elimination of PVP, which is considered an impurity, the treatment temperature must rise to at least 400 ℃.

Further possible investigations about these structured components that can be carried out are: optimising the print design, trying to make even more complex shapes, trying to modify the composition of the inks so that a continuous air jet is not required during printing to aid ink drying and analysing the actual thermal properties of the printed specimens to see whether the print design can have a positive or negative influence on heat energy storage.

Bibliography

[1] Fundamentals of Direct-Ink-Writing — Manufacturing Processes and Machinery Lab — Washington State University — labs.wsu.edu. `https://labs.wsu.edu/mpml/projects/`. [Accessed 13-10-2023].

[2] Helium pycnometer — central laboratory.

[3] Sebbe Blokhuizen. Silicon drift detector simulations for energy-dispersive x-ray spectroscopy in scanning electron microscopy, 2023.

[4] Wikipedia contributors. "shear thinning — Wikipedia the free encyclopedia", 2023. accessed 13-September-2023.

[5] Kailas Deore, Nilesh P Salunke, and Sudhakar B Pawar. Phase change materials (pcms) in solar still:-a review of use to improve productivity of still. *Materials Today: Proceedings*, 2023.

[6] Stefania Doppiu, Jean-Luc Dauvergne, Angel Serrano, and Elena Palomo del Barrio. The li2so4–na2so4 system for thermal energy storage. *Materials*, 12(22):3658, 2019.

[7] Yu Feng, Jingli Luo, and Karl T Chuang. Chemical stability of linaso4 electrolyte during operation in a h2–o2 fuel cell. *Journal of the Electrochemical Society*, 153(5):A865, 2006.

[8] Ian Gibson, David Rosen, Brent Stucker, Mahyar Khorasani, Ian Gibson, David Rosen, Brent Stucker, and Mahyar Khorasani. Material extrusion. *Additive Manufacturing Technologies*, pages 171–201, 2021.

[9] Massimo Guglielmi. Scienza e tecnologia dei materiali ceramici, dispense delle lezioni, 2016/2017.

[10] GEM Jauncey. The scattering of x-rays and bragg's law. *Proceedings of the national academy of sciences*, 10(2):57–60, 1924.

[11] M. Masera. Reologia, complementi di fisica, 2006/2007.

[12] Tuan D Ngo, Alireza Kashani, Gabriele Imbalzano, Kate TQ Nguyen, and David Hui. Additive manufacturing (3d printing): A review of materials, methods, applications and challenges. *Composites Part B: Engineering*, 143:172–196, 2018.

Bibliography

[13] John A Noël, Samer Kahwaji, Louis Desgrosseilliers, Dominic Groulx, and Mary Anne White. Phase change materials. In *Storing Energy*, pages 503–535. Elsevier, 2022.

[14] C N R Rao and B Prakash. Crystal structure transformations in inorganic sulfates, phosphates, perchlorates, and chromates:, 1975-01-01 05:01:00 1975.

[15] Eden Reid. What is Rheology? — blog.rheosense.com. `https://blog.rheosense.com/what-is-rheology`. [Accessed 08-10-2023].

[16] MASR Saadi, Alianna Maguire, Neethu T Pottackal, Md Shajedul Hoque Thakur, Maruf Md Ikram, A John Hart, Pulickel M Ajayan, and Muhammad M Rahman. Direct ink writing: a 3d printing technology for diverse materials. *Advanced Materials*, 34(28):2108855, 2022.

[17] Murat Tiryakioğlu and David Hudak. Unbiased estimates of the weibull parameters by the linear regression method. *Journal of materials science*, 43:1914–1919, 2008.

[18] Wikipedia contributors. Lithium sulfate — Wikipedia, the free encyclopedia, 2023. [Online; accessed 9-September-2023].

[19] Wikipedia contributors. Sodium sulfate — Wikipedia, the free encyclopedia. `https://en.wikipedia.org/w/index.php?title=Sodium_sulfate&oldid=1164699157`, 2023. [Online; accessed 14-September-2023].